Global application of a regional frequency analysis on extreme sea levels

Authors: Thomas P. Collings[1], Niall D. Quinn[1], Ivan D. Haigh[1,2], Joshua Green[1,2], Izzy Probyn[1], Hamish Wilkinson[1], Sanne Muis[3,4], William V. Sweet[5], Paul D. Bates[1,6]

Affiliations of Authors:

1. Fathom, Floor 2, Clifton Heights, Clifton, Bristol, UK. BS8 1EJ

2. School of Ocean and Earth Science, University of Southampton, National Oceanography Centre, European Way, Southampton SO14 3ZH

3. Deltares, Delft, Netherlands

4. Institute for Environmental Studies (IVM), Vrije Universiteit Amsterdam, Amsterdam, Netherlands

5. National Oceanic and Atmospheric Administration, National Ocean Service, Silver Spring, MD, United States

6. School of Geographical Sciences, University of Bristol, Bristol, UK

Correspondence to: t.collings@fathom.global

Abstract

Coastal regions face increasing threats from rising sea levels and extreme weather events, highlighting the urgent need for accurate assessments of coastal flood risk. This study presents a novel approach to estimating global Extreme Sea Level (ESL) exceedance probabilities, using a Regional Frequency Analysis (RFA) approach. The research combines observed and modelled hindcast data to produce a high-resolution (~1 km) dataset of ESL exceedance probabilities, including wave setup, along the entire global coastline, excluding Antarctica.

The methodology presented in this paper is an extension of the regional framework from Sweet *et al.* (2022), with innovations made to incorporate wave setup and apply the method globally. Water level records from tide gauges and a global reanalysis of tide and surge levels are integrated with a global ocean wave reanalysis. Subsequently, these data are regionalised, normalised, and aggregated, and then fit with a Generalised Pareto distribution. The regional distributions are downscaled to the local scale using the tidal range at every location along the global coastline, obtained through a global tide model. The results show 8cm of positive bias at the 1-in-10-year return level, when compared against individual tide gauges.

The RFA approach offers several advantages over traditional methods, particularly in regions with limited observational data. It overcomes the challenge of short and incomplete observational records by substituting long historical records with a collection of shorter but spatially distributed records. This spatially distributed data not only retains the volume of information but also addresses the issue of sparse tide gauge coverage in less populated areas and developing nations. The RFA process is illustrated using Cyclone Yasi (2011) as a case study, demonstrating how the approach can ~~significantly~~ improve the characterisation of ESLs in regions prone to tropical cyclone activity.

In conclusion, this study provides a valuable resource for quantifying global coastal flood risk, offering an innovative global methodology that can contribute to preparing for, and mitigating against, coastal flooding.

Plain language summary

Coastal areas are at risk of flooding from rising sea levels and extreme weather events. This study uses a new way to figure out how likely coastal flooding is around the world. The method uses data from observations and computer models to create a detailed map of where these floods might happen at the coast. The approach can predict flooding in areas where there is little or no data. The results can be used to help get ready for and prevent this type of flooding.

1. Introduction

Flooding provides one of the greatest threats to coastal communities globally, causing devastating impacts to affected regions. Notable events which have caused significant coastal flooding in recent years include: Cyclone Amphan (2020), which struck the Bay of Bengal producing a storm surge of up to 4.6m along the coast of Western Bengal, killing 84 people, and causing total losses over 13 billion USD (India Meteorological Department, 2020, Kumar *et al.*, 2021); Hurricane Harvey (2017), the second most costly hurricane to hit the US after Katrina (2005), which impacted 13 million people, hitting the state of Texas with a maximum storm surge of 3.8m (Amadeo, 2019); and Typhoon Jebi (2018), driving storm surges of over 3m in Osaka Bay, Japan, combined with wave action which led to flooding exceeding 5m above mean sea level (Mori *et al.*, 2019). Approximately 10% of the world's population (768 million people) live below 10m above mean sea level (Nicholls *et al.*, 2021). Coastal flooding is expected to increase dramatically into the future, predominantly caused by sea-level rise (Taherkhani *et al.*, 2020), and compounded by continued growth and development in coastal populations (Neumann *et al.*, 2015). Therefore, continuing to improve the understanding of coastal flooding is vital.

Coastal floods are driven by extreme sea levels, which arise as combinations of: (1) astronomical tides; (2) storm surges (driven by tropical and extra-tropical cyclones) and associated seiches; (3) waves, especially setup and runup; and (4) relative mean sea level changes (including sea-level rise and vertical land movement). Risk assessments of coastal flooding require high-quality and high-resolution flood hazard data, typically in the form of flood inundation maps. Inundation maps are usually derived from hydraulic models, which use high resolution extreme sea level (ESL) exceedance probabilities as a key input (e.g., Bates *et al.*, 2021; Mitchell *et al.*, 2022). The development of coastal inundation maps is reliant on coastal boundary conditions points that vary in resolution depending on application. Previous studies (e.g., Barnard *et al.*, 2019) have used 100m resolution at local sales, while regional studies (e.g., Bates *et al.*, 2021, Environment Agency, 2018) have employed resolutions between 500m and 2km.

Traditional methods for computing ESL exceedance probabilities involve extreme value analysis of measurements from individual tide gauges or wave buoys. However, long, complete records spanning numerous decades are necessary to obtain robust estimates of

ESL return levels (Coles, 2001). The Global Extreme Sea Level Analysis (GESLA-3) database provides sea level records for over 5,000 tide gauge stations (Haigh *et al.*, 2021), but these tide gauges still cover only a small fraction of the world's coastlines. Wave buoys are even more sparse, largely restricted to the Northern Hemisphere and long historical records are marred by discontinuities (Timmermans *et al.*, 2020). Even in areas with relatively high tide gauge or wave buoy density, there are still large expanses of coastline which remain ungauged. While rare extreme weather events (such as intense tropical cyclones (TCs)) are often many hundreds of kilometres in size, the precise impact of the corresponding ESL can often be highly localised (Irish *et al.*, 2008), meaning the peak surge occurs in an ungauged location. The particular locale of peak surge for an event is determined by storm characteristics, local bathymetry and coastal geography, amongst other factors (Shaji *et al.*, 2014). Therefore, relying on past observation-based analyses of ESL exceedance probabilities to characterise return levels across a region will likely lead to the under representation of rare extreme events. Finally, another limitation is that many previous analyses of ESL exceedance probabilities consider the still water level component (i.e., tide plus storm surge) separately from the wave set up and run up (Haigh *et al.*, 2016, Muis *et al.*, 2016, Ramakrishnan *et al.*, 2022).

One solution to overcome sparse datasets is to use ESL hindcasts created by state-of-the-art models. These include regional (e.g., (Andrée *et al.*, 2021, Siahsarani *et al.*, 2021, Tanim & Akter, 2019) or global tide-surge (such as Deltares' Global Tide Surge Model v3.0 (hereafter referred to as GTSM; Muis *et al.*, 2020) or wave models (e.g., Liang *et al.*, 2019). These are used to fill the spatial and temporal gaps in the observation records via historical reanalysis simulation. However, their ability to accurately capture extreme events is hampered by the atmospheric forcing data that is used to drive the models, as reanalysis products like ERA5 (Hersbach *et al.*, 2020) commonly contain biases in representing meteorological extremes such as ~~tropical cyclone~~TCs (Slocum *et al.*, 2022), leading to an underestimation of event intensity. Furthermore, the time period captured in reanalysis products is not adequate to represent the characteristics (e.g., frequencies) of particularly rare events such as intense ~~tropical cyclone~~TCs. To overcome this limitation, some studies have used synthetic event datasets representing ~~tropical cyclone~~TC activity over many thousands of years (e.g., Haigh *et al.*, 2014; Dullaart *et al.*, 2021), however this approach is computationally expensive.

An alternative and less computationally demanding solution that helps address some of the problems inherent in estimating ESLs around the world's coastlines from the observational record, is regional frequency analysis (RFA). The RFA methodology was originally developed to estimate streamflow within a hydrological context (e.g., Hosking and Wallis, 1997), but has since been used in many applications requiring extreme value analysis of meteorological parameters including coastal storm surge (e.g., Bardet *et al.*, 2011; Weiss and Bernardara, 2013; Arns *et al.*, 2015; Calafat *et al.* 2022) and extreme ocean waves (e.g., Campos *et al.*, 2019, Lucas *et al.*, 2017, Vanem, 2017). The principle of an RFA is founded on the basis that a homogenous region can be identified, throughout which similar meteorological forcings and resultant storm surge or wave events could occur, even if the extreme events have not been seen in part of that region in the historical record (Hosking and Wallis, 1997). RFA has been used on a regional scale to produce coastal ESL exceedance probabilities including: France (Andreevsky *et al.*, 2020, Hamdi *et al.*, 2016); the US coastline (Sweet *et al.*, 2022); Northern Europe (Frau *et al.*, 2018); US coastal military sites (Hall *et al.*, 2016); and the Pacific Basin (Sweet *et al.*, 2020). However, an RFA approach has not (to our knowledge) been applied globally.

Field Code Changed

The overall aim of this paper is to, for the first time, apply an RFA approach to estimate ESL exceedance probabilities, including wave setup, along the entire global coastline. These exceedance probabilities aim to better characterise ESLs driven by rare, extreme events, such as those from ~~tropical cyclone~~TCs, which are poorly represented in the historical record. Uniquely, this study uses both measured and hindcast datasets; includes tides, storm surges, and wave setup; and calculates exceedance probabilities at high resolution (1 km) globally. The specific objectives of this paper are to:

(1) develop and apply the RFA globally (excluding Antarctica), utilising both observational tide gauge, and modelled hindcast sea level and wave records;
(2) illustrate how the RFA methodology improves the representation of rare extreme events in the ESL exceedance probabilities using cyclone Yasi, which impacted the Australian coastline in 2011, as a case study;
(3) validate the RFA against exceedance probabilities estimated from the GESLA-3 global tide gauge database; and

(4) Finally, quantify how much the RFA ~~improves~~ increases the estimation of ESL exceedance probabilities in areas prone to TC activity when compared to single site analysis, using hindcast datasets (Muis *et al.*, 2020 and Dullaart *et al.*, 2021).

This paper is laid out as follows: The datasets used are described in Section 2. The methodology is detailed in Section 3, addressing objective 1. Results and validation are described in Section 4, addressing objectives 2, 3, and 4. A discussion of the key findings and conclusions are then given in Sections 5 and 6, respectively.

2. Data

We use seven primary sources of data in this study, namely: (1) still sea-level observations contained in the GESLA-3 tide gauge dataset; (2) global still sea-level simulations from the GTSM hindcast based on the ERA5 climate reanalysis; (3) tidal predictions from the FES2014 finite element hydrodynamic model; (4) significant wave heights derived from the ERA5 climate reanalysis; (5) mean dynamic topography from HYBRID-CNES-CLS18-CMEMS2020; (6) Copernicus DEM to create a global coastline dataset; and (7) the COAST-RP dataset from Dullaart *et al.*, (2021) to validate the RFA methodology. These seven datasets are described in turn below.

Still sea level records are assembled from the GESLA-3 (Global Extreme Sea Level Analysis) tide gauge dataset version 3 (Caldwell *et al.*, 2015, Haigh *et al.*, 2021). The GESLA-3 dataset includes high-frequency water level time series from over 5,000 tide gauges around the globe, collated from 36 international and national providers. Data providers have differing methods of quality control, however each record was visually assessed by the authors of the GESLA-3 dataset and graded as either: (i) no obvious issues; (ii) possible datum issues; (iii) possible quality control issues; or (iv) possible datum and quality control issues. Only records with no obvious issues were used in this study.

As discussed in Section 3, the hindcast, GTSM-ERA5 is used in all areas which are not covered by tide gauge observations. GTSM is a depth-averaged hydrodynamic model built using the DELFT-3D hydrodynamic model, which makes use of an unstructured, global, flexible mesh with no open boundaries (Muis *et al.*, 2020). The model has a coastal resolution of 2.5km (1.25km in Europe), and a deep ocean resolution of 25km. The GTSM-ERA5 dataset spans the period 1979-2018, and is developed by forcing GTSM with hourly fields of ERA5 10-metre wind speed and atmospheric pressure (Hersbach *et al.*, 2020). GTSM-ERA5 has a 10-minute temporal resolution and provides a timeseries at locations approximately every 50km along the coastline (10km in Europe). Validation carried out by Muis *et al*. (2020) shows that the dataset performs well against observations of annual maximum water level, exhibiting a mean bias of -0.04 m and a mean absolute percentage error of 14%.

We use the FES2014 tidal database to generate tidal timeseries at GTSM-ERA5 locations and RFA output locations. The RFA output resolution is much higher than the output resolution of GTSM-ERA5, which is why FES2014 is used instead. FES2014 is a finite element hydrodynamic model which combines data assimilation from satellite altimetry and tide gauges (Lyard *et al.*, 2021). The model solves the barotropic tidal equations, as well as the effects from self-attraction and loading. The gridded resolution of the output is 1/16°. The model was extensively validated against tide gauges, satellite altimeter observations, and alternative global tide models by Lyard *et al*. (2021) and was found to have an improved variance reduction in nearly all areas, especially in shallow water regions. The Python package distributed with the FES2014 data (https://github.com/CNES/aviso-fes) was used to simulate tidal timeseries.

To calculate wave set up we use significant wave heights (Hs) from the ERA5 reanalysis (Hersbach *et al.*, 2020), covering the period 1979 to 2020. The spatial resolution of the ERA5 wave model output is 0.5° x 0.5°, and the temporal resolution is hourly. Independent validation of hourly Hs performed by Wang & Wang (2022) finds little bias in the dataset (-0.058 m), however the authors go on to conclude that Hs of extreme waves tends to be underestimated (by 7.7% in the 95% percentile), a conclusion supported by Fanti *et al.* (2023).

We use mean dynamic topography (MDT) to convert water levels from mean sea level as measured by tide gauges to mean sea level as referenced by a geoid, for use in subsequent future studies involving inundation assessments using hydraulic modelling. MDT describes the change in sea surface height due to the effects of the winds and currents in the ocean. Digital elevation models (DEMs), a key input to hydraulic models, typically use a geoid as a vertical datum. A geoid is an equipotential surface of mean sea level under the sole effect of gravity, in the absence of land masses, currents and tides (Bingham & Haines, 2006). To convert water levels from tide gauge mean sea level to the geoid mean sea level, the HYBRID-CNES-CLS18-CMEMS2020 MDT dataset is used (Mulet *et al.*, 2021). The spatial resolution of this dataset is 0.125° x 0.125°. Errors associated with this dataset are largely caused by the input satellite altimetry data and can be up to 10 cm in some areas. The MDT at the shoreline is illustrated in the Appendix Fig. A1.

The Copernicus 30m DEM (European Space Agency, 2021) is used to create a high-resolution global coastline. This is used to define the RFA output points at approximately 1 km intervals along the global coastline (excluding Antarctica), resulting in over 3.4 million points.

Finally, in addition to GTSM-ERA5, we use the COAST-RP dataset from Dullaart *et al.* (2021) to validate the RFA methodology. COAST-RP uses the same hydraulic modelling framework as GTSM-ERA5 but simulates extra-tropical and tropical surge events separately using different forcing data. In areas prone to ~~tropical cyclone~~TC activity, synthetic ~~tropical cyclone~~TCs representing ~~10~~3,000 years under current climate conditions are used from the STORM dataset (Bloemendaal *et al.*, 2020). These synthetic ~~tropical cyclone~~TC model runs have been validated against observed IBTrACS-forced model runs, and found to show differences in ESLs at the 1 in 25 year return level of less than 0.1 m at 67% of the output locations in ~~tropical cyclone~~TC prone areas (Dullaart *et al.*, 2021). In ~~extra-tropical~~ regions impacted only by extra-tropical storms, a 38-year timeseries of ERA5 data is used (Hersbach *et al.*, 2020). The surge levels from each set of simulations are probabilistically combined with tides to result in a global database of dynamically modelled storm-tides.

3. Methods

The first objective of this study is to develop and apply an RFA approach globally, encompassing still water levels and wave set up. In Section 3.1 we describe the methods used to process the data used in this study. In Section 3.2 we layout the global application of the RFA approach using observational and modelled data. The methods used to validate the results are explained in Section 3.3.

An overview of our methodology is illustrated in Fig. 1. This study broadly follows the methodology of Sweet *et al.* (2022) and applies an RFA to both tide gauge and GTSM-ERA5 records. As such, the terms 'water level record' and 'record location' are used to describe both tide gauge records and GTSM-ERA5 data. The method can be summarised in five key steps: (i) collation and pre-processing of tide gauge, GTSM-ERA5, FES2014, and ERA5 Hs data; (ii) spatial discretisation of water level records into regions; (iii) application of the RFA to regional water level records (in areas unsuitable for an RFA (because there are less than 3 gauges in a region, or the regional water levels records are heterogenous), a peaks-over-threshold analysis of individual GTSM-ERA5 water level records is used); (iv) conversion (downscaling) of RFA exceedance levels to local exceedance levels at the output coastline points, using FES2014 tidal range (in areas unsuitable for an RFA, nearest-neighbour interpolation – is used to assign local exceedance levels); and (v) correction of bias and datums to convert water levels to geoid mean sea level, using FES2014 mean higher high water and global MDT (HYBRID-CNES-CLS18-CMEMS2020). The final section of the methods (vi) describes the validation techniques. These steps are described in detail below.

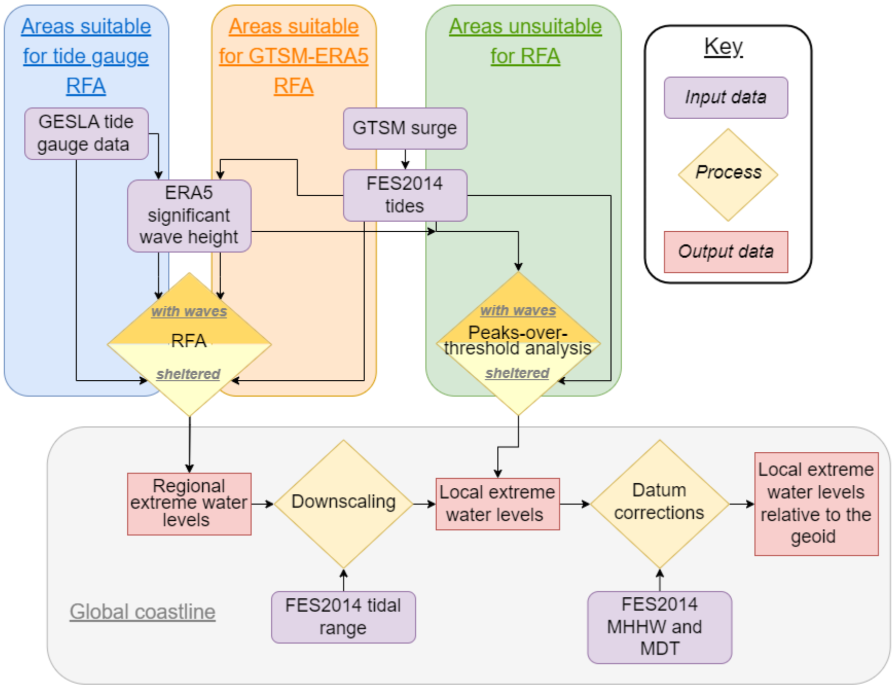

Figure 1: Schematic flow diagram detailing the data sources and processes involved in producing a global set of extreme water levels

3.1 Data processing

The GESLA-3 dataset was filtered to sample appropriate input data by removing duplicates, gauges located in rivers (away from the coast), and gauges that fail quality control checks carried out by the authors of the dataset (such as suspected datum jumps). ~~A total of 2,223 tide gauges with a mean record length of 21.4 years were used in the RFA.~~ The surge component of GTSM-ERA5 at each record location is isolated from the water level timeseries using a tide only simulation and superimposed upon a tidal timeseries created with FES2014, as the FES2014 tidal elevations performed better than those of GTSM in initial testing against in-situ observation. The decision to use tides from FES2014 is further supported by the conclusion from Muis *et al*, (2020), in which they state “It appears that biases increase in regions with a high tidal range, such as the North Sea, northern Australia, and the northwest of the United States and Canada, which could indicate that GTSM is

Formatted: Font: Not Italic

outperformed by the FES2012 model that was used to develop the GTSR dataset.” Tidal timeseries were also computed at each of the coastline output locations for use in downscaling the regional outputs, and in the bias and datum corrections of the local ESL.

Wave setup is the static increase in water level attributed to residual energy remaining after a wave breaks (Dean & Walton, 2010), and therefore is only observed in areas exposed to direct wave action. In this study, wave setup is approximated as 20% significant wave height (Hs) from the ERA5 reanalysis, following the recommendation from the review of numerous laboratory and field experiments (Dean & Walton, 2010) and previous related studies (Bates *et al.*, 2021, Vousdoukas *et al.*, 2016). Wave setup is ~~interpolated~~ assigned to the nearest record location using a nearest-neighbour approach. Wave setup is assumed to be absent in sheltered areas (e.g., bays and estuaries). To account for this~~the lack of wave setup in sheltered areas (e.g., bays and estuaries)~~, the global coastline is classified as either sheltered or exposed, and the final extreme water levels are drawn from an RFA that is processed with or without wave setup added in. To classify the coastline, each coastline point is evaluated to determine if it is exposed from a minimum 22.5° angle over a fetch of 50km. A total of 16 equal angle transects are drawn, extending 50km from each coastline point. If two or more adjacent transects do not intersect with land, the coastline point is considered exposed. Applying wave setup using this approach is an obvious simplification that has been used for the ease of global application. In reality wave setup is impacted by local bathymetry and coastal geometry, as well as local wind and wave conditions. There are other more complex methods for estimating wave setup that incorporate some aspects of bathymetry and coastal geometry, such as Stockdon et al. (2006).

To process the RFA with wave setup, daily maximum wave setup is added to the daily highest water levels. Where tide gauge records fall outside of the temporal range of the ERA5 data, a copula-based approach was used to fit a simple statistical model between daily peak water levels and daily max Hs, providing a prediction of the daily max Hs. The RFA is then executed as described below. Tide gauges are assumed to be located in sheltered regions, such as bays and estuaries, thus tide gauge records are not impacted by wave setup.

3.2 ~~RFA~~Spatial discretisation of water level records into regions

Water level records are spatially clustered to form a potential pool from which regional exceedance levels can be characterised. To do this, the global coastline is divided into 1° by 1° grid cells, which are used as the regions to apply the outputs for each RFA. All record locations within a 400km radius (same as Hall *et al.* (2016) and Sweet *et al.* (2022)) of the grid cell centroid that have at least 10 consecutive years of good (>90% completeness) data are identified (minimum of 3 water level records, maximum of 10 (same as Sweet *et al.* (2022)). This step is illustrated in Fig. 2A. Record locations which are geographically within range, but are separated by a large expanse of land, and thus likely forced by different storm patterns are removed from the record location selection. To achieve this, a line is drawn between the grid cell centroid and each record location. The land intersected by the line is divided, and the areas of land on either side of the line are summed. A ratio of the length of the line to the area of land segmented by the line is then calculated. A threshold of 100 was empirically evaluated using expert judgement based on a number of test cases, above which records are removed from the grid cell analysis. This approach ensures that, for example, record locations located on the east coast of Florida (e.g., Mayport) are not grouped with those on the west coast (e.g., Cedar Key) when characterising regional growth curves, despite the relatively short straight-line distance between them. Fig. 2A exemplifies three tide gauges which have been excluded from possible selection despite lying within a 400km radius to the grid cell centroid as the land that separates them is considerably large when compared to the distance. This spatial discretisation of regions results in a total of 836 tide gauge records (with a mean record length of 17 years) and 18628 GTSM-ERA5 records for use in the application of the RFA.

Formatted: Font: Italic

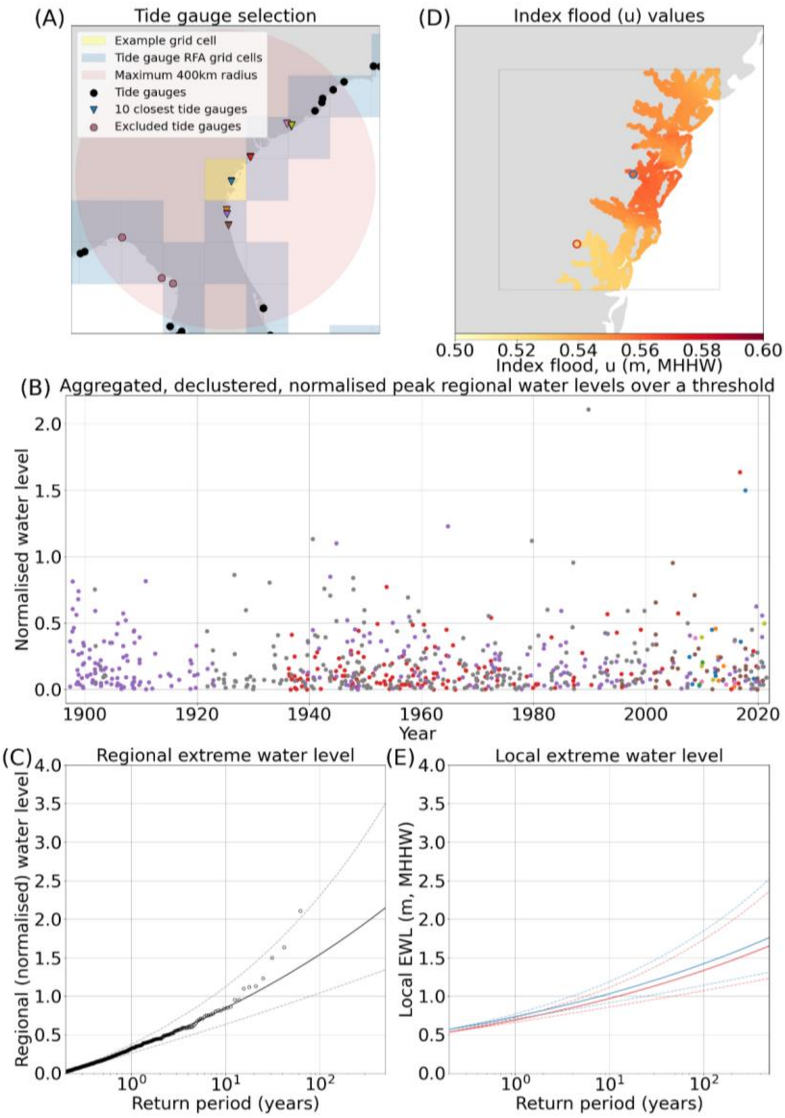
(A)
Tide gauge selection
Example grid cell
Tide gauge RFA grid cells
Maximum 400km radius
Tide gauges
10 closest tide gauges
Excluded tide gauges
(D)
Index flood (u) values
0.50
0.52
0.54
0.56
0.58
0.60
Index flood, u (m, MHHW)
(B)
Aggregated, declustered, normalised peak regional water levels over a threshold
Normalised water level
0.0
0.5
1.0
1.5
2.0
1900
1920
1940
1960
1980
2000
2020
Year
(C)
Regional extreme water level
Regional (normalised) water level
0.0
0.5
1.0
1.5
2.0
2.5
3.0
3.5
4.0
Return period (years)
(E)
Local extreme water level
Local EWL (m, MHHW)
Return period (years)

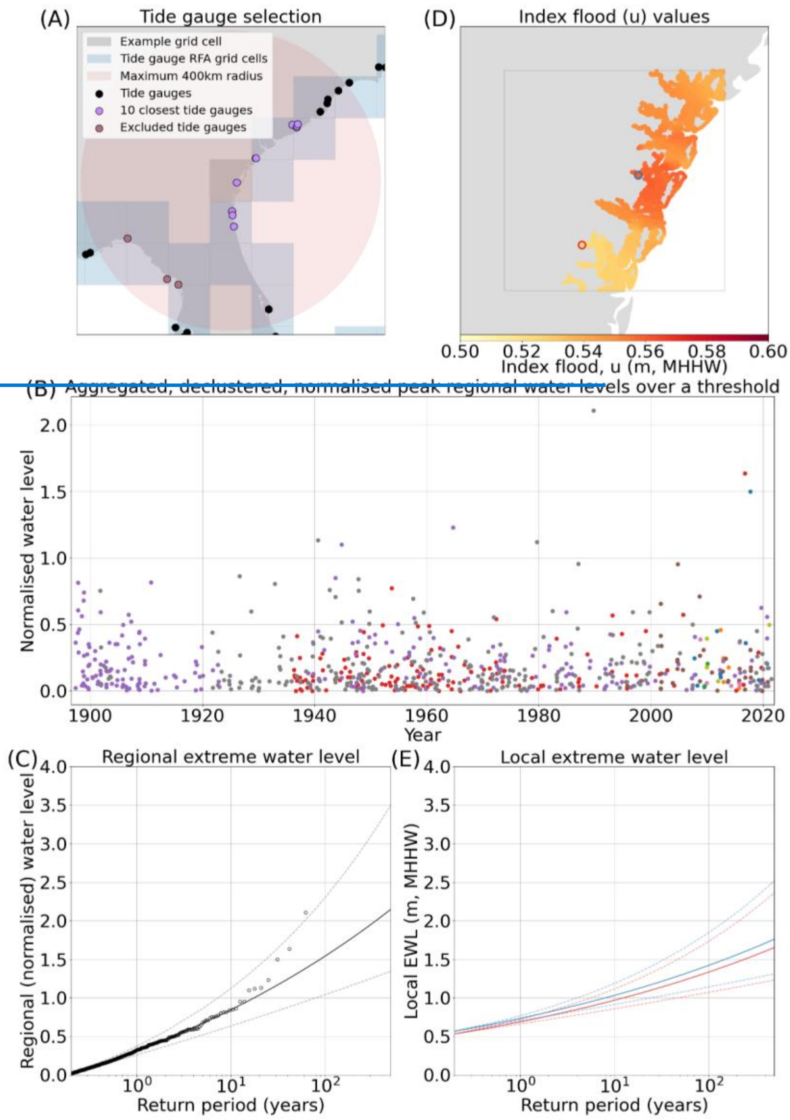

Figure 2: Illustrating a selection of the steps through the RFA. (A) The 1° by 1° grid cells along the East Coast of the US, along with the locations of the tide gauges, and the tide gauges selected for the RFA of the example grid cell. The tide gauges excluded from possible selection by the distance/land area ratio are also indicated. (B) The aggregated, declustered, normalised peak regional water levels over a threshold for each of the tide gauges used in the example grid cell. The colours indicate peak water levels from the individual tide gauges in the region. (C) The regional extreme water levels, ascertained by fitting a Generalised Pareto distribution to the data displayed in panel (B). (D) The index flood values of the example grid cell, found by linearly interpolating the u value from the two closest tide gauges, and scaling by tidal range. The locations of two coastline points used to produce local extreme water levels in panel E are also highlighted. (E) The local extreme water level at two shoreline points inside the example grid cell, each with different index flood values as indicated in panel D.

The RFA is preferentially applied to tide gauges in areas where the gauge density is sufficient (minimum 3 gauges within a 400km radius, same as Hall *et al.* (2016) and Sweet *et al.* (2022)). Outside of these areas, the RFA is implemented using data from GTSM-ERA5. In some regions, the density of homogenous record locations from GTSM-ERA5 is also too low for the RFA to function, in which case the ESL exceedance probabilities are interpolated from a single site peaks-over-threshold analysis of the nearest GTSM-ERA5 record location. The geographical locations of these areas are shown in Fig. 3. From the 5,975 global coastal grid cells, ESLs at 851 are computed using tide gauge data, 4,555 are calculated using an RFA of GTSM-ERA5 data, and 569 are calculated using GTSM-ERA5 data from the nearest record location.

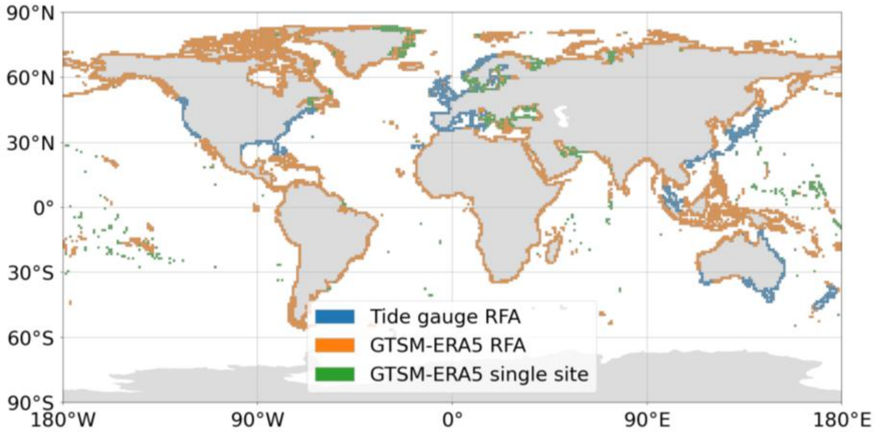

Figure 3: This map shows the global distribution the areas in which the tide gauge RFA is used, the GTSM-ERA5 RFA is used, and the areas which are interpolations of single site analysis from GTSM-ERA5.

3.3 Application of the RFA

~~Water level~~Tide gauge records are referenced to different vertical datums, so to ensure consistency, the mean over the most recent 19-year epoch is subtract from the water level record, and the timeseries is linearly detrended to the centre year of the most recent available epoch (2002-2020), resulting in 2011. GTSM-ERA5 records are referenced to MSL over the period of 1986-2005, and so the timeseries are linearly detrended to reference the same tidal epoch as the tide gauge records, centred on 2011. Within each cluster of gauge

Formatted: Font: 14 pt, Bold

Formatted: Line spacing: Multiple 1.08 li (or model) records, the water level time series are resampled to hourly resolution and converted to mean higher high water, defined as the mean daily highest water level over a 19-year epoch, to account for differences in tidal range between record locations. In the case of records with fewer than 19 years of data available the maximum continuous epoch is used instead.

Daily highest water level is determined from the hourly time series of each measured or modelled record. The time series are then declustered using a 4-day ~~moving window of the storm~~storm window to ensure event independence. This window length~~-~~ was used by Sweet *et al.*, 2020 and Sweet *et al.*, 2022, and is a similar length to the storms that cause surge events in the UK ~~was selected as storms that cause surge events are known to last approximately 4 days~~ (Haigh *et al.*, 2016). The index flood u, defined as the 98th percentile of the declustered daily highest water levels (Sweet *et al.*, 2022), is used as the exceedance threshold at which to normalise the water level at each record location, as follows:

$$Normalised\ water\ level = (Observed\ exceedence\ water\ level - u)\ /u \qquad \text{(eq. 1)}$$

The normalised datasets are then aggregated and further declustered to ensure only one peak water level is retained for each regional event. This is shown in Fig. 2B for an example grid cell. Following Hosking and Wallis (1997), a statistical heterogeneity test (H) is undertaken to ensure the homogeneity of the region. If the H-score is less than 2, then the region is considered sufficiently homogenous. If the H-score is greater than 2, then the furthest water level record from the grid cell centroid is removed from the region, and the test re-run. This process is repeated until the H-score is less than 2. In a minority of cases, the heterogeneity test fails due to an anomalous record that lies within the closest 3 sampling locations to the grid cell centroid. In this instance the test is rerun, except after the furthest record is removed, all the remaining records are sequentially removed and replaced, until the H-score is less than 2.

After the region is confirmed to be homogenous, a Generalised Pareto distribution is fitted to the aggregated, declustered, normalised regional water levels using a penalised maximum likelihood method to estimate regional extreme water levels (REWLs). This is illustrated at an example in Fig. 2C. This is repeated for the aggregated regional water levels for each 1° by 1° grid cell. While theoretically correct, applying distribution fits to real world

Formatted: No underline

data can sometimes give unrealistic results, particularly in the estimation of the lower frequency space. In these cases, growth curve optimisation is undertaken to ensure the output local extreme water levels are plausible in real world scenarios. To ensure consistency, an empirical threshold of 0.35 for the shape parameter is used to determine which curves will generate unrealistic extreme water levels. The empirical threshold of the shape parameter is determined based on expert judgement of plausible real world maximum surge heights in the low frequency events. To correct these curves, where this threshold is exceeded, we use the shape and scale parameters of the nearest grid cell which has a shape parameter less than 0.35. In total, 34 grid cells had their shape and scale parameters adjusted, mostly concentrated in the Gulf of Mexico and Japan.

3.4 Downscaling to local extreme water levels

Formatted: Font: 14 pt, Bold

Formatted: Line spacing: Multiple 1.08 li

Local extreme water levels (LEWLs) are then estimated from the regional growth curves using the following relationship:

$$LEWL = (REWL * u) + u \qquad \text{(eq. 2)}$$

for each coastal point along the coastline contained within the grid cell represented by the REWL. The index u is estimated at the coastline points using an inverse distance weighting interpolation of the u values for the two closest record locations, scaled by tidal range. This deviates from the methodology set out by Sweet *et al.* (2022), in which they recommend drawing u values from a linear regression of u against tidal range values from record locations across a region. We found this approach led to significant differences in LEWLs at record locations when compared to single site analysis of water level records, and hence have modified the methodology. Fig. 2D exhibits an example of the index flood for every shoreline point in an example grid cell. Tidal ranges are calculated as the difference between mean higher high water and mean lower low water. Tidal harmonics from FES2014 are used to predict mean higher high water and mean lower low water at each coastline point. The index flood, u, is used to downscale the REWLs, which represent the ESL characteristics of the entire grid cell. LEWLs are output in the format of return levels for a range of exceedance probabilities. Two example LEWL curves are shown in Fig. 2E, which have been computed using different index flood values, as indicated in Fig. 2D. ~~The index flood, u, is used to downscale the REWLs, which represent the ESL characteristics of the~~

~~entire grid cell. LEWLs are output in the format of return levels for a range of exceedance probabilities. The index u is then estimated at the coastline points using an inverse distance weighting interpolation of the u values for the two closest record locations, scaled by tidal range. This deviates from the methodology set out by Sweet *et al.* (2022), in which they recommend drawing u values from a linear regression of u against tidal range values from record locations across a region. We found this approach led to significant differences in LEWLs at record locations when compared to single site analysis of water level records, and hence have modified the methodology. Fig. 2D exhibits an example of the index flood for every shoreline point in an example grid cell. Tidal ranges are calculated as the difference between mean higher high water and mean lower low water. Tidal harmonics from FES2014 are used to predict mean higher high water and mean lower low water at each coastline point.~~

3.5 Bias and datum corrections

The last stage of the LEWL calculation involved characterisation and removal of bias in the high frequency portion of the exceedance probability curves, relative to ~~the~~ a single site analysis of water level records (within which we expect the high frequency water levels to be accurately modelled). Other surge RFA studies also concluded that the approach generally yields higher estimated surge heights when compared to single site analysis, because during the regionalisation process an extreme event that occurred in one location is assumed to have the same probability of occurring at another location within the homogeneous region. (Bardet *et al.*, *2011; Sweet et al., 2022).* Bias is quantified based on the divergence in the 1-in-1-year return period at each tide gauge/GTSM-ERA5 location and the corresponding LEWL predictions. This bias is used as a correction term and is removed from the LEWLs. As the density of the coastline points is much greater than the density of the tide gauges/model output locations, the correction term is interpolated across all coastal LEWL points based on correlation between ~~Q99~~ monthly values of the 99th percentile of tidal elevations produced over a 3-year period centred on 2011, ~~tidal elevations~~ computed using FES2014 at the tide gauge/GTSM-ERA5 location and neighbouring coastline points. The mean bias correction across all gauges is 8 cm.

Formatted: Font: 14 pt, Bold

Formatted: Line spacing: Multiple 1.08 li

Formatted: Superscript

Datum corrections are applied to ensure the LEWLs are correctly referenced to a vertical datum which can be used for hazard assessment applications, such as inundation modelling. Inundation models utilise digital elevation models, which typically reference a geoid as the vertical datum. The output water levels from the RFA are transformed from mean higher high water to Mean Sea Level (MSL) by adding the approximation of mean higher high water (above MSL) from the FES2014 simulations to each of the boundary condition points. The corrected MDT dataset from (Mulet *et al.*, 2021) is applied to convert water levels from MSL from the FES2014 model to the ‘MSL’ of a commonly used geoid, EGM08.

3.6~~3~~ Validation methods

In this section we define a range of validation techniques used to address objectives 3 and 4. To validate the RFA ESLs against tide gauge records from GESLA (objective 3), a comparison is made against ESL exceedance probabilities calculated at the individual tide gauges used to inform the RFA. To quantify the degree to which the RFA approach improves the estimation of ESL exceedance probabilities compared to single site analysis (objective 4), two assessments are made.

Firstly, the divergence between GTSM-ERA5 RFA ESL and GTSM-ERA5 single site ESL for the entire global coastline are quantified. These are then contrasted against the differences between return levels from GTSM-ERA5 (Muis *et al.*, 2020) and COAST-RP (Dullaart *et al.* 2021). ~~GTSM-ERA5 is forced with 39 years of ERA5 data, a relatively short period when considering exceedance probabilities for rare extreme events (e.g., tropical cyclones). To overcome this data paucity, GTSM was subsequently run with STORM~~ a database containing ~~10,000 years of synthetic storm tracks (Bloemendaal *et al.*, 2020).~~ ~~resulting in COAST-RP, a database containing 10,000 years of synthetic storm tracks (Bloemendaal *et al.*, 2020).~~ The comparison can then identify regions in which the historical ESLs are poorly represented due to the limited record lengths.

Secondly, a leave-one-out cross validation is undertaken using GTSM-ERA5 data. Leave-one out-cross validation aims to address the common issues involved with validating statistical models. One common method to validate models is split-sample validation, in which the data is split into two groups, a training set and a validation set, which are generally 70% and 30% of the data respectively. The model is then trained on the larger set and validated against the smaller set. The drawbacks of this method include a highly variable validation error, due to the selection of the training and validation sets, as well as a validation error bias caused by training the model on only 70% of the available data (James *et al.*, 2013).

Instead of using a 70/30 split of the data, leave-one-out cross validation uses a larger proportion of the data to train the model, while validating against a smaller sub-sample, but repeats this process multiple times to generate a robust validation. ~~In this study,~~To do this, we identified 1000 grid cells which ~~have~~ use 10 GTSM-ERA5 records ~~used~~ for the RFA and contain 3 GTSM-ERA5 record locations inside the grid cell (and therefore the RFA can be used to directly estimate ESLs at the record locations)~~are identified~~. One of the GTSM-ERA5 records from inside the grid cell is removed from the RFA process, and the REWL is calculated using the 9 remaining gauges. The LEWL is then predicted at the record location which has been left out, using the index flood, u at the record location. These LEWLs are then contrasted with a single site analysis of the water level record that was removed from the RFA. The process is then repeated for the 2 other GTSM-ERA5 record locations which lie within the grid cell. This means each of the 1000 models is being tested three times, against 90% of the available data, thus giving a more robust realisation of the model when trained on 100% of the data.

4. Results

The results section is divided into four sub-sections. Section 4.1 presents the results of the global application of the RFA, showing both the global view of two return periods and the return levels for selected sites around the world. Section 4.2 illustrates how the RFA methodology improves the characterisation of rare extreme events using Cyclone Yasi (objective 2). In section 4.3 we validate the RFA against estimates of ESL from GESLA tide gauges (objective 3). Finally, in section 4.4 we quantify the improvements made by using an RFA approach when compared to a single site analysis of water levels (objective 4).

4.1 Global application of RFA

The final ESL exceedance probabilities (including wave setup) created at high resolution around the global coastline are displayed in Fig. 4, for the 1-in-10 and 1-in-100-year return periods. Both the 1-in-10 year (Fig. 4A) and 1-in-100 year (Fig. 4B) return periods show similar spatial patterns, with 1-in-100-year return periods exhibiting greater increases as expected in areas prone to ~~tropical cyclone~~TC activity (e.g., the Gulf of Mexico, Australia, Japan, and China). ESLs are higher in regions with large tidal ranges such as the Bay of Fundy, the Patagonia Shelf, the Bristol Channel in UK, the northern coast of France, and the northwest coast of Australia. The return levels for 6 select tide gauge locations, 3 of which are characterised by a positive and 3 of which are characterised by negative shape parameter from the Generalised Pareto distribution are shown in Fig. 4C and 4D respectively, relative to mean higher high water. The locations of the 6 tide gauges are indicated in both Fig. 4A and 4B. Regions exhibiting positive shape parameters are typically prone to ~~tropical cyclone~~TC activity and associated surge and wave events. As a result, these regions experience more significant increases in return levels at higher return periods than regions with negative shape parameters. Regions characterised by negative shape parameters have different drivers of ESL events, for instance extra-tropical storms surges or tide dominated ESLs (Sweet *et al.*, 2020).

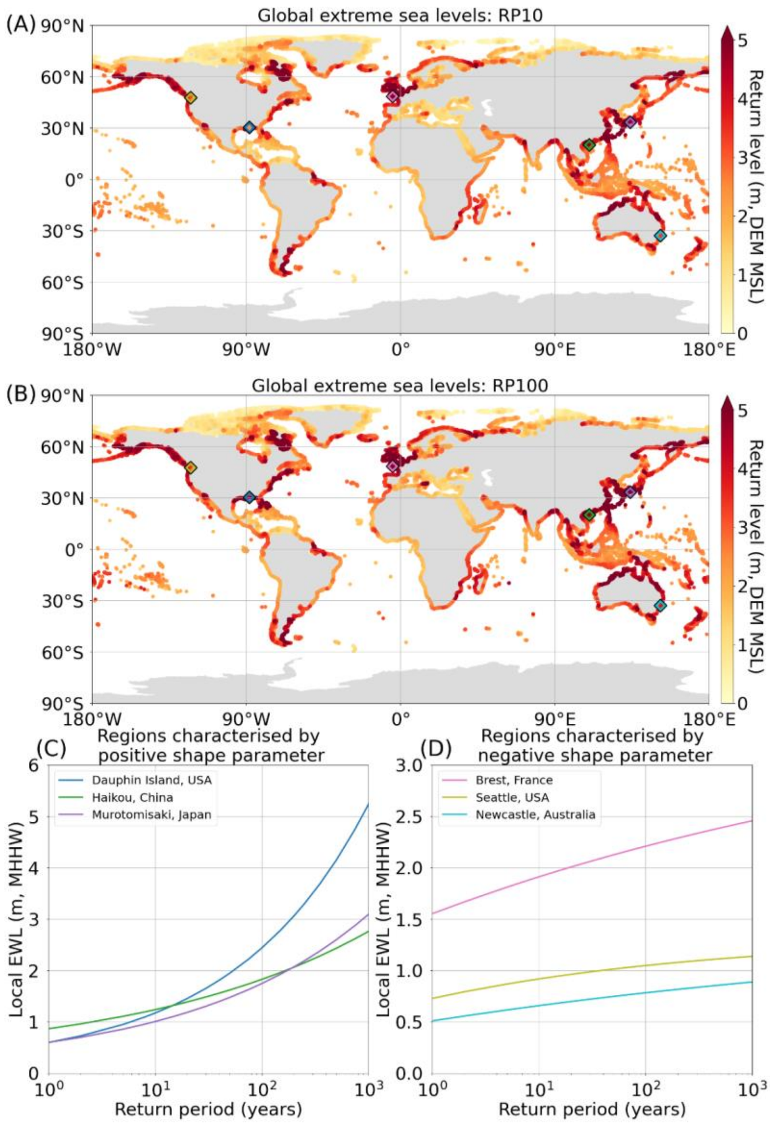

Figure 4: The final global RFA results output at approximately 1km resolution along the entire global coastline (excluding Antarctica) for RP10 (A) and RP100 (B). Return levels are referenced to DEM MSL, and so represent surge, waves and tide. Return levels (relative to mean higher high water) for 6 tide gauges in regions characterised by either positive or negative shape parameter of the Generalised Pareto distribution are shown in panels (C) and (D) respectively. The locations of the 6 tide gauges are indicated by the diamonds plotted on both panels (A) and (B).

4.2 Tropical Cyclone Yasi

Our second study objective is to illustrate how the RFA methodology ~~improves the representation of rare extreme events~~previously described can draw on few, rare events, to provide more realistic representation of low frequency ~~in the~~ ESL exceedance probabilities across a region, using the case study of cyclone Yasi which impacted the Australian coastline in 2011.~~ As demonstrated in this study, one major advantage the RFA approach benefits from is its capacity to capture the extreme rare events that are typically under sampled in historical records.~~ Cyclone Yasi made landfall on the North-eastern coast of Australia, in the Queensland region, between 14:00 and 15:00 UTC on the 2nd of February 2011. It is the strongest cyclone to have impacted the region since 1918, with possible windspeeds of 285km/h and minimum record pressure centre of 929 hPa (Australia Bureau of Meteorology, 2011). When it made landfall, Yasi was a category 4 storm on the Saffir-Sampson scale. The path and strength of the storm are shown in Fig. 5A.

The total water levels, relative to mean higher high water, for all the tide gauges in the region are shown in Fig. 5~~4~~B. Cardwell had the highest surge, and highest total water level, by a considerable margin compared to neighbouring tide gauges, receiving a surge of over 3m above mean higher high water. Clump Point also showed a definitive but less substantial surge signal, whereas the other gauges showed much smaller surge effects or even no surge at all. The historical water level records of all the gauges in the regions are included in Fig. 5C. The tide gauges span different temporal ranges, and many have years which are incomplete. The longest record is at Townsville, which started in the late 1950s. Despite this record, the largest event is cyclone Yasi by over 1.5m (at Cardwell).

~~Cardwell is not unique in location. The width of the continental shelf is reasonably constant throughout this section of coastline, and while the position of the tide gauge is located towards the back of a semi-enclosed bay, any local effects due to surge (from bathymetry or coastline shape) will be accounted for by normalising the data using the index flood.~~ Based on this historical record, no other ~~major~~ surge event of this magnitude has impacted this section of coastline since the records began. There are, however, records of other historic extreme events that predate tide gauges affecting the region. For example, Cyclone Mahina, which made landfall in Princess Charlotte Bay (approximately 100km north of Cooktown) in 1899, reportedly had a surge height approaching 10m (Needham *et al.*, 2015). The idea that this stretch of coastline is at risk of ~~tropical cyclone~~TC generated ESLs is further supported by STORM, a dataset of 10,000 years of synthetic hurricane tracks (Bloemendaal *et al.*, 2020). IBTrACS shows just eight category 4 and 5 hurricanes impacting this 700km stretch of coastline between 1980 and 2022 (shown in the Appendix Fig. A2; Knapp *et al.*, 2010). In contrast, the STORM dataset has 333 events affecting the area, producing a more continuous spread of landfall locations along the coastline. In addition, large surges are sometimes not captured in this region due to the lack of gauges in rural areas (Needham *et al.*, 2015).

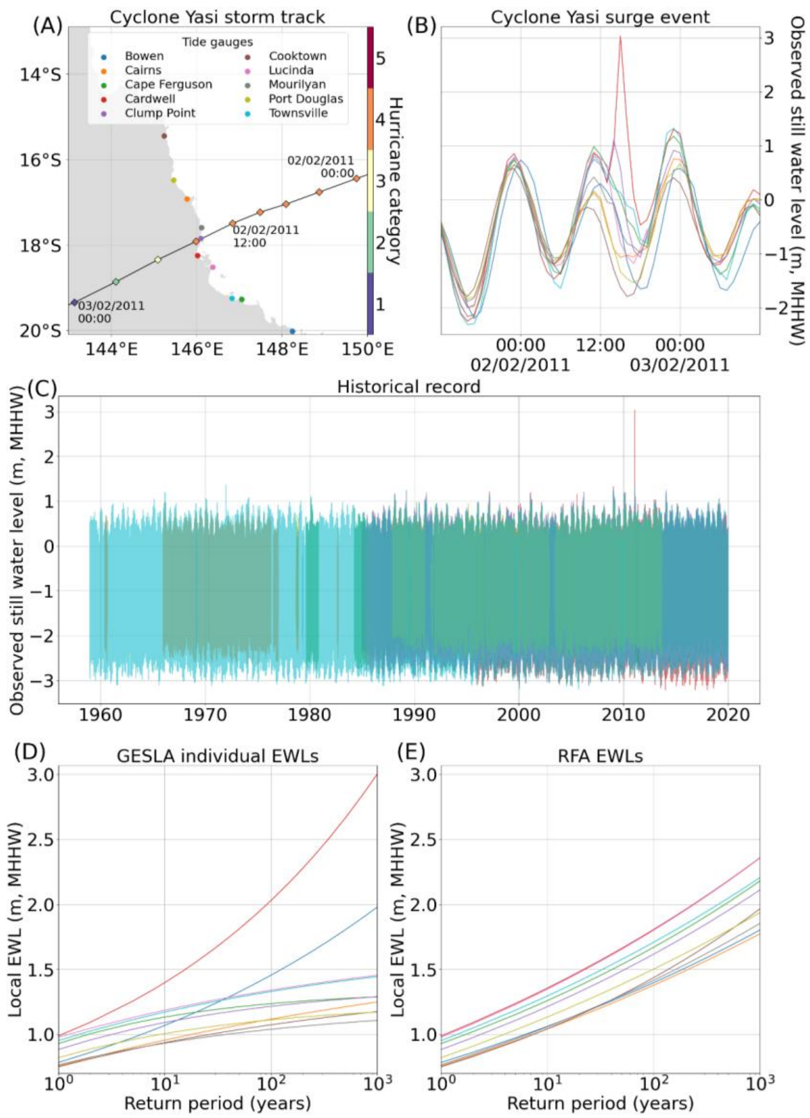

Figure 5: Tropical Cyclone Yasi: (A) The storm track of cyclone Yasi, covering a 24-hour period over the landfall event. The locations of the 10 closest tide gauges along the Queensland coast are also included. Times are in UTC. (B) The observed water level timeseries for the same 24-hour period at each of the 10 tide gauges in the region. Times are in UTC. (C) The entire historical record of all 10 gauges in the region. (D) The return period curves of individual gauges fit with Generalised Pareto distribution. (E) The return period curves at the gauge locations from the RFA.

The return period curves, calculated by fitting a Generalised Pareto distribution to the peaks-over-threshold water levels at each individual tide gauge, for each of the 10 gauges in the region, are shown in Fig. 5D. As expected, Cardwell has the largest return levels and the steepest curve. All the other gauges, except Bowen, exhibit negative shape parameters, characterised by a decreasing gradient of the return period curves. In a region which is prone to ~~tropical cyclone~~TCs, this is a dangerous underestimation of the risk from cyclone induced surges. In some coastal ESL studies, ESLs are calculated at each gauge, and then interpolated along the coastline, such as in the UK (Environment Agency, 2018). In this case, that approach would lead to a gross disparity from the actual risk of storm surges to coastal communities in the area.

In contrast, Fig. 5E shows the return period curves estimated from the RFA at the tide gauge locations. All of the curves now have positive shape parameters, characterised by increasing gradients of the curves. The curves of Cardwell and Bowen have been reduced somewhat, while all the other curves have been increased significantly. This demonstrates the regionalisation process, by which the extreme event at Cardwell can be used to propagate the risk along the coastline to areas which have not had an extreme event on record, or have short, incomplete, or non-existent tide gauge records. This reinforces the key strengths of the RFA, namely: (1) the ability to spatially account for rare extreme events, (2) the use of short and incomplete tide gauge records to produce robust parameter fits, and (3) the ability to downscale the results into regions which aren't covered by tide gauges at all.

4.3 Comparisons with GESLA

The third objective is to validate ESLs calculated using our RFA against those calculated directly from the measured GESLA-3 global tide gauge database. Contrasting the RFA results with ESL exceedance probabilities calculated through a Generalised Pareto distribution fit at individual tide gauges yields promising results. Fig. 6A shows the spatial distribution of the difference at the 1-in-10-year return period for Europe, the United States, and the East Pacific. In areas impacted by ~~tropical cyclone~~TCs (e.g., the Gulf of Mexico, North-Eastern Coast of Australia, and Japan) we broadly see that the RFA has increasing return levels across most gauges. Increases in the 1-in-10-year return level are also observed in areas usually associated with extra-tropical storms (e.g., Europe), suggesting gauges in these regions also suffer from under sampling of rare surge events. Extreme surge events can be undersampled for two reasons. Firstly, by their very nature, they are rare and might never have occurred at a specific location. Secondly, as a result of a scarcity of in-situ tide gauges, surges can occur and remain unrecorded.

In all areas shown in Figure 6A, some gauges show decreases in the return levels. This could be driven by either shape parameter limiting (to prevent unrealistically large water levels), an anomalously large number of events impacting the gauge, or due to a single anomalously large event impacting the gauge, which is then smoothed out through the regionalisation process, as was the case in Cardwell, Australia (Fig. 5E). Of the gauges shown in the Fig. 6A, only 5 had limited shape parameters, which were located in the Gulf of Mexico. The distribution of the differences at RP10 is shown in Fig. 6B with a positive skew, detailing the 5th and 95th percentiles as -8cm and 27cm respectively. The spread of the data increases across the three selected return periods (1-in-2, 1-in-10 and 1-in-100 year) presented in in Fig. 6C, as well as the mean bias, which increased from 2 cm in the 1-in-2 year return level, to 21cm in the 1-in-100 year return level.

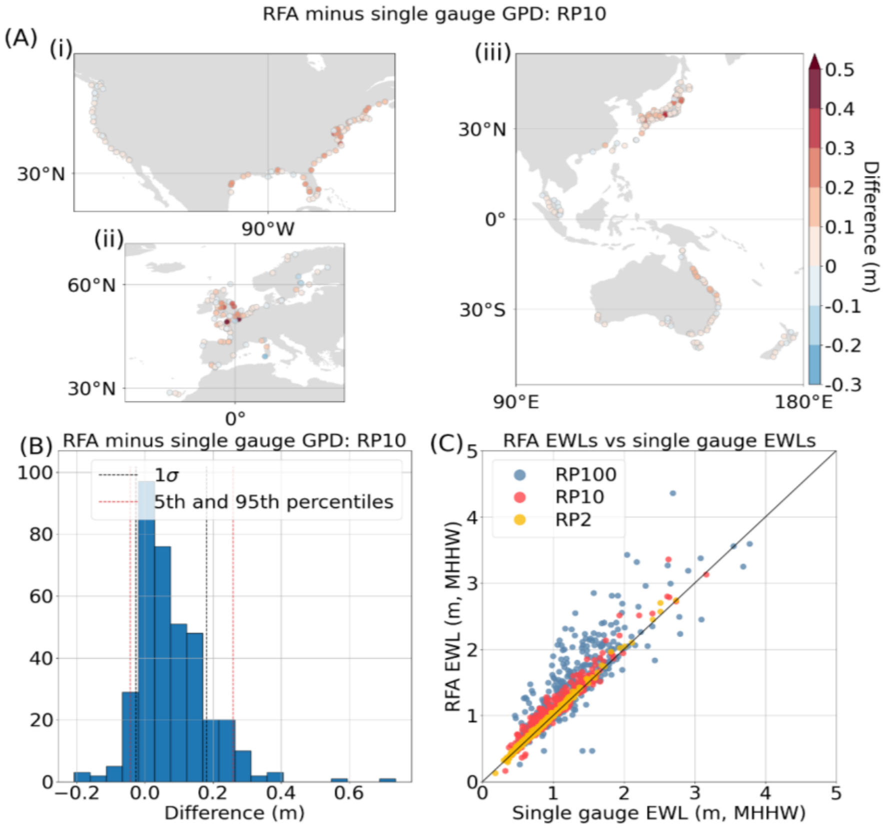

Figure 6: Comparison of RFA water levels against extreme water levels calculated at individual gauges from GESLA by fitting a Generalised Pareto distribution to peaks-over-threshold water levels. (A) The spatial distribution of the difference at RP10 for (i) the contiguous US, (ii) Europe, (iii) Japan, Malaysia, Australia and New Zealand, (B) a histogram of the distributions of difference at RP10, including the locations of the 5th and 95th percentiles and 1 standard deviation from the mean, and (C) a scatter plot of EWLs (RP2, RP10, RP100) from the RFA and the EWLs calculated using a single site Generalised Pareto distribution fit. The black line indicates a 1:1 perfect fit.

4.4 Quantifying the ~~improvements~~ increases made by the RFA when compared to single site analysis

The fourth objective is to quantify the ~~improvements~~ increases made to ESL exceedance probabilities in TC prone areas by the RFA, when compared to a single site analysis. Figure 7A shows the deviation in the 1-in-100-year return period between the GTSM-ERA5 RFA carried out across the global coastline, and a single site peaks-over-threshold analysis of GTSM-ERA5 water level records. Only differences greater or less than 0.25 m and -0.25 m respectively, are plotted. There are evident increases to RFA ESLs in areas prone to ~~tropical cyclone~~TCs. The Gulf of Mexico, the East Coast of the US, Southern China, and the North-East Coast of Australia show the largest increases. Sporadic negative differences are also observed in Fig. 7A, which are driven ~~by an over-sampling of extreme events at these record locations, and subsequent reduction in ESL exceedance probabilities by the RFA~~by a smoothing of ESL exceedance probabilities at locations which have experienced anomalously high ESL compared to the local region. From this we see that the RFA is capable of incorporating the influence of ~~tropical cyclone~~TCs that were not present in the historical record, but statistically could occur as indicated by the regional characteristic.

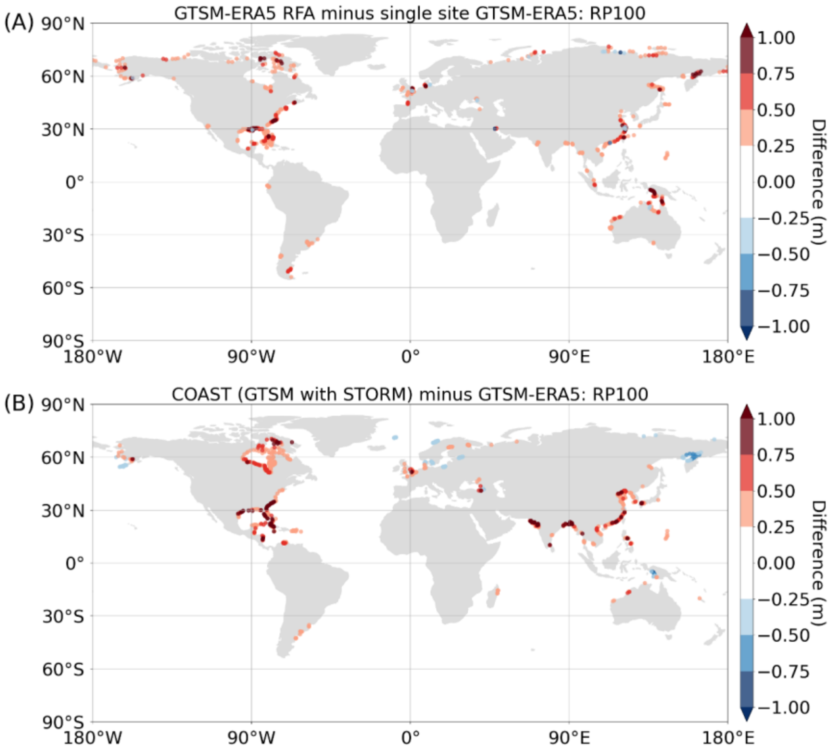

Figure 7: The spatial distributions of: (A) the differences between the GTSM-ERA5 RFA 1-in-100-year return period (RP100) and the RP100 of single site GTSM-ERA5 data fit with a Generalised Pareto distribution to the peaks-over-threshold water

levels; and (B) the differences in RP100 published by the COAST-RP (GTSM forced with STORM) paper (Dullaart et al., 2021) and RP100 published by the original GTSM paper (Muis et al., 2020). Only differences greater or less than 0.25 m and -0.25 m, respectively, are plotted.

These findings can be supported by the results shown in Fig. 7B, which shows the differences between COAST-RP and GTSM-ERA5. COAST-RP is GTSM forced with STORM (10,000 years of synthetic ~~tropical cyclone~~TCs) in areas prone to ~~tropical cyclone~~TC activity, instead of ERA5 (Dullaart *et al.*, 2021). The areas of positive difference highlight locations where COAST-RP is greater than GTSM-ERA5, and so give an indication of the areas in which the synthetic hurricanes make landfall. These patterns are broadly similar to those of the RFA, shown in Fig. 7A. However, there are two areas which stand out for being poorly characterised by the RFA, namely: the Bay of Bengal and the western Gujarat region of India. Large differences are also observed in Hudson Bay, Canada, however we suspect these discrepancies are the result of differences in the approach to modelling extra-tropical regions, as ~~tropical cyclone~~TCs do not make landfall here.

Figure 8 shows the results of the leave-one-out cross validation of the global coastal LEWLs. In general, the RFA tends to increase return levels due to the regionalisation process. These findings match those of (Sweet *et al.*, 2020, Sweet *et al.*, 2022) upon which our approach is based. This is evident throughout the world, with the majority of gauges exhibiting increases of less than 5 cm at the 1-in-10-year return period (Fig. 8A). The central 90th percentile band of the data for the 1-in-10-year return period ranges from -3 to 18 cm, as shown in Fig. 8B. However, the spread of the data is more pronounced at the higher return periods, as shown in Fig. 8C. Some regions of the world have greater increases, in the order of 30 – 40 cm for the 1-in-10 year return period. These gauges are mostly concentrated in ~~tropical cyclone~~TC basins, namely the Caribbean, the Gulf of Mexico, Japan, China, the Philippines, plus the East and West Coasts of Australia. This demonstrates the process by which the RFA better represents extreme rare events that are typically under ~~-~~sampled in the historical record. By drawing on all the events captured by gauges across the region, the RFA reveals that there is greater risk of extreme events by considering their potential occurrence in areas that, by chance, have not been previously impacted as observed in historical records. Similarly, oversampling is clearly evident at 1-in-100-year return periods, for which nearly a third of locations show decreases in ESL exceedance probabilities compared to the single site analysis. The magnitude of these decreases tend to be much smaller than the increases seen.

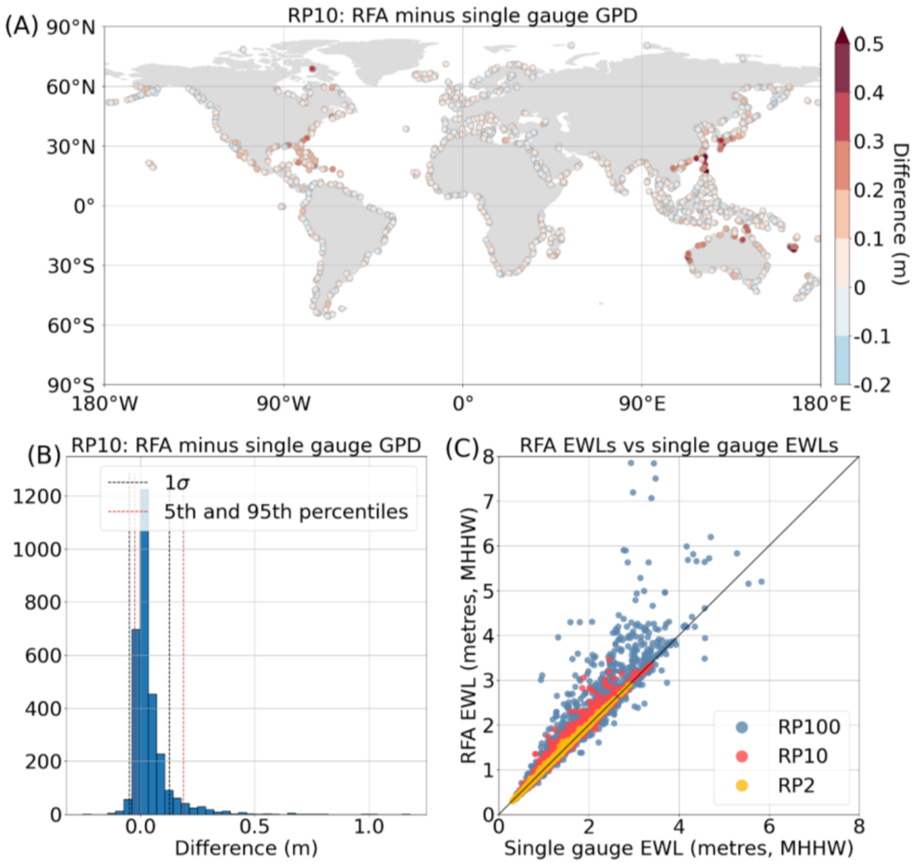

Figure 8: The results of the leave-one-out cross validation of the RFA on GTSM-ERA5 gauges. (A) The spatial distribution of difference between the leave-one-out cross validation RFA RP10 (1 in 10-year return period) and the single site Generalised Pareto distribution RP10, (B) a histogram of the distribution of the differences in RP10 including the locations of the 5th and 95th percentiles and 1 standard deviation from the mean, and (C) a scatter plot of EWLs (RP2, RP10, and RP100) predicted using the leave-one-out cross validation RFA and the EWLs calculated using a single site Generalised Pareto distribution fit. The black line indicates a 1:1 perfect fit.

5. Discussion

The ESL exceedance probabilities dataset that is presented in this paper is the first global dataset, to our knowledge, to be derived using an RFA approach, using a synthesis of observed and modelled hindcast data. The resulting data is output at high resolution (~1 km) along the entire global coastline (excluding Antarctica), includes wave setup, and better captures the coastal flood risk from ~~tropical cyclone~~TCs. This approach is notable for being computationally inexpensive compared to more traditional approaches for deriving ESL exceedance probabilities via hydrodynamic modelling.

As previously discussed in the introduction section, relying solely on observational records to estimate ESL exceedance probabilities can significantly bias results. To fit robust parameter estimates and obtain confident exceedance probabilities sufficient for informing flood risk managers, long term and consistent high quality observational records are needed (Coles, 2001). While some tide gauge and wave records span numerous decades, many records only cover a handful of recent decades (e.g., 10-30 years) or have significant gaps in their historical records. This often means quality data is excluded from analyses as their records are too short to produce robust parameter estimates. Furthermore, gauges are relatively sparse, especially in less populated areas and developing nations. While surges and waves typically impact large regions, peak water levels are usually only observed over smaller areas (i.e., a single bay, estuary or beach). As a result, measured records can easily miss the maximum of an extreme event, thus mischaracterising extreme water levels ~~at the gauge~~of the event. As such, rare extreme events that characterise the upmost tails of the distributions of ESLs, such as ~~tropical cyclone~~TCs, are repeatedly under sampled in the historic record, in both frequency and magnitude.

By using an RFA approach, we demonstrate how we have ~~overcome~~ improved these issues. The RFA can be viewed as a space-for-time approach, where long historical records (which give robust parameter estimates) are substituted for a collection of shorter records that cover a larger area. The volume of data (and subsequent extreme events) is retained, but the individual records can be much shorter. In this study, records as short as 10 years have been utilised. Furthermore, the regionalisation process works to overcome the issues with gauge density by disseminating the hazard presented by rare extreme events, as shown using the Cyclone Yasi example. From the 10 gauges in the region, the only record to have captured an historic extreme surge event of the magnitude observed during Cyclone Yasi was Cardwell, despite this section of coastline being at known risk to ~~tropical cyclone~~TC activity. A single site analysis of tide gauge data in this region would ~~woefully~~ likely underpredict the real risk of ESLs generated by ~~tropical cyclone~~TCs in areas which haven't had a direct impact in the observational record. On the other hand, the damping of the return levels in the RFA output at Cardwell and Bowen could mean an underprediction of the risk from surges in these locations.

Global hydrodynamic models that simulate tide and surge (e.g., GTSM) or waves have been developed to substitute observational records, especially in regions not covered by tide gauges. These models have been demonstrated to represent historic extreme events to a high degree ~~t~~of accuracy when forced using historical observational data pertaining to the event (Yang *et al.*, 2020). However, using these models for the characterisation of exceedance probabilities is limited by the availability of long term high-quality global reanalysis data, that captures the full extent of meteorological extremes that drive large surge events. ~~Once again, the RFA provides a solution to this problem~~The RFA is aims to address this by using a space-for-time approach, however it is still limited by the bounds of the GTSM-ERA5 data. ~~.~~As demonstrated in Fig. 7, the distribution of increases to local return levels made by the RFA broadly follows the same patterns globally as the differences between COAST-RP and GTSM-ERA5. As TC hazard is typically underrepresented due to short records, it can be inferred that the increases observed across these regions are an improvement on a single site analysis. ~~This highlights the ability of the RFA to characterise tropical cyclone hazard which is typically underrepresented as a result of short records.~~

While the RFA is capable of identifying areas of increased risk from ~~tropical cyclone~~TC activity, it is still constrained by the training data available. This is demonstrated in Fig. 7. Two distinct areas lack increased water levels in the RFA difference plot (Fig. 7A), namely: the Bay of Bengal and Northwestern coasts of India and Pakistan. ERA5, the forcing data used for GTSM-ERA5~~The model hindcast, GTSM-ERA5, only covers the relatively short period of 1979-2018.~~ has been found to consistently underestimate TC intensity in both minimum sea level pressure and maximum windspeed (Dulac *et al.*, 2023). Consequently, the intensity of extreme events in GTSM-ERA5 in these regions ~~does not accurately~~could under-represent

Field Code Changed

the potential hazard from ~~tropical cyclone~~TC activity. If the maximums of extremes are not captured in the reanalysis data, then the full magnitude of the surge cannot be simulated by GTSM-ERA5. As such, the RFA ~~has little basis upon~~will have smaller or fewer extremes with which to draw data from when characterising rare extreme events, therefore leading to a persistent underestimation of the return levels.

Coastal flood hazard mapping is usually carried out using inundation models that simulate the propagation of water over the coastal floodplain. To accurately capture the footprint of the surge on the land, inundation models require high-resolution boundary conditions at regular intervals along the coastline. The density of boundary condition points needs to be sufficient to capture local variability in ESLs along a coastline, which can be caused by bathymetric and topographic features such as narrow channels, enclosed bays, barrier island and estuaries. The spatial resolution of tide gauges, even in the areas of highest gauge density, is insufficient for direct use in inundation modelling and therefore requires some form of interpolation and/or extrapolation. Similarly, while GTSM-ERA5, is run at a reasonably high coastal resolution, publicly available data is only output at approximately 50km resolution outside of Europe, and therefore does not meet the standards necessary for coastal floodplain inundation modelling. Using the RFA to downscale the regional extreme water levels allows for the possibility of implementing tide gauge data and the outputs from GTSM-ERA5 as boundary conditions for subsequent inundation models. In addition, the downscaling process involves scaling the water levels by tidal range and thus enables dynamic characteristics of the surge, such as amplification at the head of estuaries, to be reproduced in the inundation models. This downscaling process is, however, limited by the resolution of the tide model used to obtain the tidal range values. In the case of this study, FES2014 is output at $1/16^{th}$ of a degree (approximately 7km at the equator).

Formatted: Superscript

Ultimately, the future of delineating the flood hazard from ~~tropical cyclone~~TCs lies in multi-ensemble models using 100's of 1,000's of years' worth of synthetically generated storms forcing high-resolution tide-surge-wave models. However, the computational cost of running such simulations is enormous when compared to the cost of running an RFA on a relatively short hindcast record. In the same way, dynamically modelled waves are usually excluded from global simulations that consider exceedance probabilities due to the computational expense. At the same time, failing to considering the joint dependence of surge and waves can lead to an underestimation of ESL exceedance levels by up to a factor of two along 30% of the global coastline (Marcos *et al.*, 2019). This reinforces the significance of the RFA methodology in characterising global coastal flood risk.

Validating the RFA is nuanced, as assessing metrics compared with observed record is: (a) validating against the data used to build the RFA in the first place; and (b) not recognising the inadequacies of the tide gauge records that the RFA is attempting to mitigate. Leave-one-out cross validation highlights the strengths of the RFA, without succumbing to the shortfalls inherent in the observational record. The increased LEWLs in the regions prone to ~~tropical cyclone~~TC activity once again demonstrates the RFA's ability to spatially disperse the hazard of low probability extreme events across a region. It is worth noting that the leave-one-out cross validation is the best possible representation of the RFA as only grid cells that use data from 10 record locations are used, so each model is trained on the maximum amount of data possible. In some areas, the number of records used can be as low as three, and so the ability for the RFA to reproduce water levels in these regions could be compromised.

Applying the RFA as done in this study does have its limitations. Firstly, changing our definition of a homogeneous region would likely have a great impact on our results. In future iterations of this study, we recommend carrying out a sensitivity analysis to understand how using different maximum radii to select water level records impacts upon estimated extreme water levels within the region. Secondly, d~~D~~elineating the global coastline into 1° by 1° tiles and evaluating a different RFA for each tile results in some complex areas of coastline being summarised by a single regional growth function. Examples of this are seen in Japan, where exposed coastlines of the North Coast are contained in the same tile as a sheltered bay that is open to the South Coast. ~~-~~A solution to this would be to classify coastlines based on descriptors, as carried out by Sweet *et al.* (2020). These descriptors could include characteristics such as dominant forcing type, geographic location, and/or local coastal dynamics. The method used to incorporate wave setup is another constraint, as it has been greatly simplified for ease of global application. Improving upon this should also be a focus of future studies. ~~-~~Lastly, another limitation of the approach used in this study is the static shape parameter limiter. It is probable that the maximum shape parameter varies by location around the world, and that by implementing a fixed threshold globally we are perhaps limiting some of the most extreme events in some regions. Improving this section of the methodology is a high priority for future updates.

The outputs from the RFA should be supplemented with local knowledge wherever possible, and the uncertainties in the results should be considered before the data is used. The RFA is a powerful tool for estimating return levels in ungauged locations or in locations where the historical records are short or incomplete, but there are risks associated with both overpredicting and underpredicting surge heights. Underprediction can lead to complacency among coastal managers and the potentially dangerous assumption that communities are safe from surge risk. Conversely, overprediction can result in unnecessary cost for risk mitigation measures and potential economic loss driven by a lack of investment in a region deemed at risk. Disseminating the risk of TC generated surges over a region could lead to overprediction in some locations, and so conducting sensitivity analyses to understand the robustness of findings is recommended, especially in the context of coastal management and safety assessments. The RFA has been developed in this study as a method for regional to continental to global scale risk analyses from globally available data, and not local studies. The results give a first order approximation of extreme water levels in ungauged locations. It is not expected that they would be used in the design for local flood defences, for example.

Going forward, the RFA framework developed in this study can be easily updated with the availability of new data. Possible next steps could also include using GTSM simulations of future climate scenarios, as well as measured wave data. To this end, a global wave dataset similar to GESLA would be instrumental in collating wave data from the numerous buoys globally. Future updates could also include an assessment of using different extreme value distributions, perhaps following the mixed climate approach of O'Grady *et al.*, (2022).

Formatted: Font: Italic

In the near future, we plan to use the global exceedance probabilities derived in this paper as boundary conditions for inundation modelling of the coastal floodplain of the entire globe, using the 2D hydraulic model LISFLOOD-FP (Bates *et al.*, 2010). This presents an exciting opportunity to provide an invaluable resource that will help to better quantify global coastal flood risk.

6. Conclusions

In this paper we have demonstrated an RFA approach utilising both measured and modelled hindcast records to estimate ESL exceedance probabilities, including wave setup, at high resolution (~1 km) along the entire global coastline (with the exception of Antarctica). Our methodology is computationally inexpensive and is more effective in accurately estimating the low frequency exceedance probabilities that are associated with rare extreme events, compared to approaches that consider data from single sites. We have demonstrated, using Cyclone Yasi (2011) which impacted the Australia coast, the ability of the RFA to better characterise ESLs in regions prone to ~~tropical cyclone~~TC activity. Furthermore, on the global scale we have exemplified how the RFA, when trained on relatively short reanalysis data, can reproduce patterns of increased water levels similar to those present in dynamic simulations of 10,000 years of synthetic hurricane tracks. The RFA methodology shown provides a promising avenue for improving our understanding of coastal flooding and enhancing our ability to prepare for and mitigate its devastating impacts. In the future, we plan to use the exceedance probabilities from this study as boundary conditions for an inundation model covering the global coastal floodplain.

7. References

Amadeo, K. (2019) Hurricane Harvey Facts , Damage and Costs. Retrieved from https://www.lamar.edu/_files/documents/resilience-recovery/grant/recovery-and-resiliency/hurric2.pdf

Andrée, E., Su, J., Larsen, M. A. D., Madsen, K. S. & Drews, M. (2021) Simulating major storm surge events in a complex coastal region. *Ocean Model.* **162**. doi:10.1016/j.ocemod.2021.101802

Andreevsky, M., Hamdi, Y., Griolet, S., Bernardara, P. & Frau, R. (2020) Regional frequency analysis of extreme storm surges using the extremogram approach. *Nat. Hazards Earth Syst. Sci.* **20**(6). doi:10.5194/nhess-20-1705-2020

Arns, A., Wahl, T., Haigh, I. D. & Jensen, J. (2015) Determining return water levels at ungauged coastal sites: a case study for northern Germany. *Ocean Dyn.* **65**(4). doi:10.1007/s10236-015-0814-1

Australia Bureau of Meteorology. (2011) Severe Tropical Cyclone Yasi. Retrieved from http://www.bom.gov.au/cyclone/history/yasi.shtml

Bardet, L., Duluc, C. M., Rebour, V. & L'Her, J. (2011) Regional frequency analysis of extreme storm surges along the French coast. *Nat. Hazards Earth Syst. Sci.* **11**(6). doi:10.5194/nhess-11-1627-2011

Barnard, P. L., Erikson, L. H., Foxgrover, A. C., Hart, J. A. F., Limber, P., O'Neill, A. C., Ormondt, M. van, et al. (2019) Dynamic flood modeling essential to assess the coastal impacts of climate change. *Sci. Rep.* **9**(1). doi:10.1038/s41598-019-40742-z

Bates, P. D., Horritt, M. S. & Fewtrell, T. J. (2010) A simple inertial formulation of the shallow water equations for efficient two-dimensional flood inundation modelling. *J. Hydrol.* **387**(1–2). doi:10.1016/j.jhydrol.2010.03.027

Bates, P. D., Quinn, N., Sampson, C., Smith, A., Wing, O., Sosa, J., Savage, J., et al. (2021) Combined Modeling of US Fluvial, Pluvial, and Coastal Flood Hazard Under Current and Future Climates. *Water Resour. Res.* **57**(2). doi:10.1029/2020WR028673

Bingham, R. J. & Haines, K. (2006) Mean dynamic topography: Intercomparisons and errors. *Philos. Trans. R. Soc. A Math. Phys. Eng. Sci.* **364**(1841). doi:10.1098/rsta.2006.1745

Bloemendaal, N., Haigh, I. D., Moel, H. de, Muis, S., Haarsma, R. J. & Aerts, J. C. J. H. (2020) Generation of a global synthetic tropical cyclone hazard dataset using STORM. *Sci. Data* **7**(1). doi:10.1038/s41597-020-0381-2

Calafat, F. M., Wahl, T., Tadesse, M. G. & Sparrow, S. N. (2022) Trends in Europe storm surge extremes match the rate of sea-level rise. *Nature* **603**(7903). doi:10.1038/s41586-022-04426-5

Caldwell, P. C., Merrifield, M. A. & Thompson, P. R. (2015) Sea level measured by tide gauges from global oceans — the Joint Archive for Sea Level holdings (NCEI Accession 0019568), Version 5.5. *NOAA Natl. Centers Environ. Inf.* (18).

Campos, R. M., Guedes Soares, C., Alves, J. H. G. M., Parente, C. E. & Guimaraes, L. G. (2019) Regional long-term extreme wave analysis using hindcast data from the South Atlantic Ocean. *Ocean Eng.* **179**. doi:10.1016/j.oceaneng.2019.03.023

Coles, S. (2001) *An Introduction to Statistical Modeling of Extreme Values*. Bristol: Springer.

Formatted: Font: (Default) Calibri, 11 pt

Formatted: Space After: 8 pt, Line spacing: single

Dean, R. & Walton, T. (2010) Wave Setup. In: *Handbook of Coastal and Ocean Engineering*, 1st ed., Vol. 1–2, 1–24. World Scientific Publishing co. doi:10.1142/10353

Dulac, W., Cattiaux, J., Chauvin, F., Bourdin, S. & Fromang, S. (2023) Assessing the representation of tropical cyclones in ERA5 with the CNRM tracker. *Clim. Dyn.* doi:10.1007/s00382-023-06902-8

Dullaart, J. C. M., Muis, S., Bloemendaal, N., Chertova, M. V., Couasnon, A. & Aerts, J. C. J. H. (2021) Accounting for tropical cyclones more than doubles the global population exposed to low-probability coastal flooding. *Commun. Earth Environ.* **2**(1). doi:10.1038/s43247-021-00204-9

Environment Agency. (2018) Coastal flood boundary conditions for the UK: 2018 update. Retrieved from https://www.gov.uk/government/publications/coastal-flood-boundary-conditions-for-uk-mainland-and-islands-design-sea-levels

European Space Agency. (2021) Copernicus Global Digital Elevation Model. *Open Topol.* 1. doi:doi.org/10.5069/G9028PQB

Fanti, V., Ferreira, Ó., Kümmerer, V. & Loureiro, C. (2023) Improved estimates of extreme wave conditions in coastal areas from calibrated global reanalyses. *Commun. Earth Environ.* **4**(1). doi:10.1038/s43247-023-00819-0

Frau, R., Andreewsky, M. & Bernardara, P. (2018) The use of historical information for regional frequency analysis of extreme skew surge. *Nat. Hazards Earth Syst. Sci.* **18**(3). doi:10.5194/nhess-18-949-2018

Haigh, I D, Marcos, M., Talke, S. A., Woodworth, P. L., Hunter, J. R., Hague, B. S., Bradshaw, E., et al. (2021) GESLA Version 3: Amajor update to the global higher-frequency sea-level dataset. *EarthArXiv* (released), 1–34. Retrieved from https://www.gesla.org.

Haigh, Ivan D., MacPherson, L. R., Mason, M. S., Wijeratne, E. M. S., Pattiaratchi, C. B., Crompton, R. P. & George, S. (2014) Estimating present day extreme water level exceedance probabilities around the coastline of Australia: Tropical cyclone-induced storm surges. *Clim. Dyn.* **42**(1–2). doi:10.1007/s00382-012-1653-0

Haigh, Ivan D., Wadey, M. P., Wahl, T., Ozsoy, O., Nicholls, R. J., Brown, J. M., Horsburgh, K., et al. (2016) Spatial and temporal analysis of extreme sea level and storm surge events around the coastline of the UK. *Sci. Data*. doi:10.1038/sdata.2016.107

Hall, J. A., Gill, S., Obeysekera, J., Sweet, W., Knuuti, K. & Marburger, J. (2016) Regional Sea Level Scenarios for Coastal Risk Management : Managing the Uncertainty of Future Sea Level Change and Extreme Water Levels for Department of Defense Coastal Sites Worldwide (April), 224. Retrieved from https://apps.dtic.mil/sti/citations/AD1013613

Hamdi, Y., Duluc, C. M., Bardet, L. & Rebour, V. (2016) Use of the spatial extremogram to form a homogeneous region centered on a target site for the regional frequency analysis of extreme storm surges. *Int. J. Saf. Secur. Eng.* **6**(4). doi:10.2495/SAFE-V6-N4-777-781

Hersbach, H., Bell, B., Berrisford, P., Hirahara, S., Horányi, A., Muñoz-Sabater, J., Nicolas, J., et al. (2020) The ERA5 global reanalysis. *Q. J. R. Meteorol. Soc.* **146**(730), 1999–2049. John Wiley & Sons, Ltd. doi:https://doi.org/10.1002/qj.3803

Hosking, J. R. M. & Wallis, J. R. (1997) *Regional Frequency Analysis: An approach based on L-moments, Cambridge University Press, New York.* Cambridge Universtiy Press. doi:https://doi.org/10.1017/CBO9780511529443

India Meteorological Department. (2020) Super Cyclonic Storm Amphan over the southeast Bay of Bengal: Summary. Retrieved from https://internal.imd.gov.in/press_release/20200614_pr_840.pdf

Irish, J. L., Resio, D. T. & Ratcliff, J. J. (2008) The influence of storm size on hurricane surge. *J. Phys. Oceanogr.* **38**(9). doi:10.1175/2008JPO3727.1

James, G., Witten, D., Hastie, T. & Tibshirani, R. (2013) *An Introduction to Statistical Learning*. Springer. doi:10.1007/9781461471387

Knapp, K. R., Kruk, M. C., Levinson, D. H., Diamond, H. J. & Neumann, C. J. (2010) The international best track archive for climate stewardship (IBTrACS). *Bull. Am. Meteorol. Soc.* **91**(3). doi:10.1175/2009BAMS2755.1

Kumar, S., Lal, P. & Kumar, A. (2021) Influence of Super Cyclone "Amphan" in the Indian Subcontinent amid COVID-19 Pandemic. *Remote Sens. Earth Syst. Sci.* **4**(1–2). doi:10.1007/s41976-021-00048-z

Liang, B., Gao, H. & Shao, Z. (2019) Characteristics of global waves based on the third-generation wave model SWAN. *Mar. Struct.* **64**. doi:10.1016/j.marstruc.2018.10.011

Lucas, C., Muraleedharan, G. & Guedes Soares, C. (2017) Regional frequency analysis of extreme waves in a coastal area. *Coast. Eng.* **126**. doi:10.1016/j.coastaleng.2017.06.002

Lyard, F. H., Allain, D. J., Cancet, M., Carrère, L. & Picot, N. (2021) FES2014 global ocean tide atlas: Design and performance. *Ocean Sci.* **17**(3), 615–649. doi:10.5194/os-17-615-2021

Marcos, M., Rohmer, J., Vousdoukas, M. I., Mentaschi, L., Cozannet, G. Le & Amores, A. (2019) Increased Extreme Coastal Water Levels Due to the Combined Action of Storm Surges and Wind Waves. *Geophys. Res. Lett.* **46**(8). doi:10.1029/2019GL082599

McGranahan, G., Balk, D. & Anderson, B. (2007) The rising tide: Assessing the risks of climate change and human settlements in low elevation coastal zones. *Environ. Urban.* **19**(1). doi:10.1177/0956247807076960

Mitchell, D., Hawker, L., Savage, J., Bingham, R., Lord, N. S., Khan, M. J. U., Bates, P., et al. (2022) Increased population exposure to Amphan-scale cyclones under future climates. *Clim. Resil. Sustain.* **1**(2), 1–16. doi:10.1002/cli2.36

Mori, N., Yasuda, T., Arikawa, T., Kataoka, T., Nakajo, S., Suzuki, K., Yamanaka, Y., et al. (2019) 2018 Typhoon Jebi post-event survey of coastal damage in the Kansai region, Japan. *Coast. Eng. J.* **61**(3). doi:10.1080/21664250.2019.1619253

Muis, S., Apecechea, M. I., Dullaart, J., Lima Rego, J. de, Madsen, K. S., Su, J., Yan, K., et al. (2020) A High-Resolution Global Dataset of Extreme Sea Levels, Tides, and Storm Surges, Including Future Projections. *Front. Mar. Sci.* **7**(April), 1–15. doi:10.3389/fmars.2020.00263

Muis, S., Verlaan, M., Winsemius, H. C., Aerts, J. C. J. H. & Ward, P. J. (2016) A global reanalysis of storm surges and extreme sea levels. *Nat. Commun.* **7**(1), 11969. doi:10.1038/ncomms11969

Mulet, S., Rio, M. H., Etienne, H., Artana, C., Cancet, M., Dibarboure, G., Feng, H., et al. (2021) The new CNES-CLS18 global mean dynamic topography. *Ocean Sci.* **17**(3), 789–808. doi:10.5194/os-17-789-2021

Needham, H. F., Keim, B. D. & Sathiaraj, D. (2015) A review of tropical cyclone-generated storm surges: Global data sources, observations, and impacts. *Rev. Geophys.* **53**(2), 545–591. doi:10.1002/2014RG000477

Neumann, B., Vafeidis, A. T., Zimmermann, J. & Nicholls, R. J. (2015) Future coastal population growth and exposure to sea-level rise and coastal flooding - A global assessment. *PLoS One*

10(3). doi:10.1371/journal.pone.0118571

Nicholls, R. J., Lincke, D., Hinkel, J., Brown, S., Vafeidis, A. T., Meyssignac, B., Hanson, S. E., et al. (2021) A global analysis of subsidence, relative sea-level change and coastal flood exposure. *Nat. Clim. Chang.* **11**(4). doi:10.1038/s41558-021-00993-z

O'Grady, J. G., Stephenson, A. G. & McInnes, K. L. (2022) Gauging mixed climate extreme value distributions in tropical cyclone regions. *Sci. Rep.* **12**(1). doi:10.1038/s41598-022-08382-y

Ramakrishnan, R., Remya, P. G., Mandal, A., Mohanty, P., Arayakandy, P., Mahendra, R. S. & Nair, T. M. B. (2022) Wave induced coastal flooding along the southwest coast of India during tropical cyclone Tauktae. *Sci. Rep.* **12**(1). doi:10.1038/s41598-022-24557-z

Shaji, C., Kar, S. K. & Vishal, T. (2014) Storm surge studies in the North Indian Ocean: A review. *Indian J. Mar. Sci.* **43**(2).

Siahsarani, A., Karami Khaniki, A., Aliakbari Bidokhti, A. A. & Azadi, M. (2021) Numerical Modeling of Tropical Cyclone-Induced Storm Surge in the Gulf of Oman Using a Storm Surge–Wave–Tide Coupled Model. *Ocean Sci. J.* **56**(3). doi:10.1007/s12601-021-00027-x

Slocum, C. J., Razin, M. N., Knaff, J. A. & Stow, J. P. (2022) Does ERA5 mark a new era for resolving the tropical cyclone environment? *J. Clim.* 1–39. doi:10.1175/jcli-d-22-0127.1

Sweet, W. V., Hamlington, B. D., Kopp, R. E., Weaver, C. P., Barnard, P. L., Bekaert, D., Brooks, W., et al. (2022) Global and Regional Sea Level Rise Scenarios for the United States. *NOAA Tech. Rep. NOS 01* 111 pp. Retrieved from https://oceanservice.noaa.gov/hazards/sealevelrise/noaa-nos-

Sweet, W. V, Genz, A. S., Obeysekera, J. & Marra, J. J. (2020) A Regional Frequency Analysis of Tide Gauges to Assess Pacific Coast Flood Risk . *Front. Mar. Sci.* . Retrieved from https://www.frontiersin.org/articles/10.3389/fmars.2020.581769

Taherkhani, M., Vitousek, S., Barnard, P. L., Frazer, N., Anderson, T. R. & Fletcher, C. H. (2020) Sea-level rise exponentially increases coastal flood frequency. *Sci. Rep.* **10**(1). doi:10.1038/s41598-020-62188-4

Tanim, A. H. & Akter, A. (2019) Storm-surge modelling for cyclone Mora in the northern Bay of Bengal. *Proc. Inst. Civ. Eng. Marit. Eng.* **172**(3). doi:10.1680/jmaen.2019.1

Timmermans, B. W., Gommenginger, C. P., Dodet, G. & Bidlot, J. R. (2020) Global Wave Height Trends and Variability from New Multimission Satellite Altimeter Products, Reanalyses, and Wave Buoys. *Geophys. Res. Lett.* **47**(9). doi:10.1029/2019GL086880

Vanem, E. (2017) A regional extreme value analysis of ocean waves in a changing climate. *Ocean Eng.* **144**. doi:10.1016/j.oceaneng.2017.08.027

Vousdoukas, M. I., Voukouvalas, E., Mentaschi, L., Dottori, F., Giardino, A., Bouziotas, D., Bianchi, A., et al. (2016) Developments in large-scale coastal flood hazard mapping. *Nat. Hazards Earth Syst. Sci.* **16**(8). doi:10.5194/nhess-16-1841-2016

Wang, J. & Wang, Y. (2022) Evaluation of the ERA5 Significant Wave Height against NDBC Buoy Data from 1979 to 2019. *Mar. Geod.* **45**(2). doi:10.1080/01490419.2021.2011502

Weiss, J. & Bernardara, P. (2013) Comparison of local indices for regional frequency analysis with an application to extreme skew surges. *Water Resour. Res.* **49**(5). doi:10.1002/wrcr.20225

Yang, Z., Wang, T., Castrucci, L. & Miller, I. (2020) Modeling assessment of storm surge in the Salish Sea. *Estuar. Coast. Shelf Sci.* **238**. doi:10.1016/j.ecss.2019.106552

~~Amadeo, K. (2019) Hurricane Harvey Facts , Damage and Costs. Retrieved from https://www.lamar.edu/_files/documents/resilience-recovery/grant/recovery-and-resiliency/hurric2.pdf~~

~~Andrée, E., Su, J., Larsen, M. A. D., Madsen, K. S. & Drews, M. (2021) Simulating major storm surge events in a complex coastal region. *Ocean Model.* **162**. doi:10.1016/j.ocemod.2021.101802~~

~~Andreevsky, M., Hamdi, Y., Griolet, S., Bernardara, P. & Frau, R. (2020) Regional frequency analysis of extreme storm surges using the extremogram approach. *Nat. Hazards Earth Syst. Sci.* **20**(6). doi:10.5194/nhess-20-1705-2020~~

~~Arns, A., Wahl, T., Haigh, I. D. & Jensen, J. (2015) Determining return water levels at ungauged coastal sites: a case study for northern Germany. *Ocean Dyn.* **65**(4). doi:10.1007/s10236-015-0814-1~~

~~Australia Bureau of Meteorology. (2011) Severe Tropical Cyclone Yasi. Retrieved from http://www.bom.gov.au/cyclone/history/yasi.shtml~~

~~Bardet, L., Duluc, C. M., Rebour, V. & L'Her, J. (2011) Regional frequency analysis of extreme storm surges along the French coast. *Nat. Hazards Earth Syst. Sci.* **11**(6). doi:10.5194/nhess-11-1627-2011~~

~~Barnard, P. L., Erikson, L. H., Foxgrover, A. C., Hart, J. A. F., Limber, P., O'Neill, A. C., Ormondt, M. van, et al. (2019) Dynamic flood modeling essential to assess the coastal impacts of climate change. *Sci. Rep.* **9**(1). doi:10.1038/s41598-019-40742-z~~

~~Bates, P. D., Horritt, M. S. & Fewtrell, T. J. (2010) A simple inertial formulation of the shallow water equations for efficient two-dimensional flood inundation modelling. *J. Hydrol.* **387**(1–2). doi:10.1016/j.jhydrol.2010.03.027~~

~~Bates, P. D., Quinn, N., Sampson, C., Smith, A., Wing, O., Sosa, J., Savage, J., et al. (2021) Combined Modeling of US Fluvial, Pluvial, and Coastal Flood Hazard Under Current and Future Climates. *Water Resour. Res.* **57**(2). doi:10.1029/2020WR028673~~

~~Bingham, R. J. & Haines, K. (2006) Mean dynamic topography: Intercomparisons and errors. *Philos. Trans. R. Soc. A Math. Phys. Eng. Sci.* **364**(1841). doi:10.1098/rsta.2006.1745~~

~~Bloemendaal, N., Haigh, I. D., Moel, H. de, Muis, S., Haarsma, R. J. & Aerts, J. C. J. H. (2020) Generation of a global synthetic tropical cyclone hazard dataset using STORM. *Sci. Data* **7**(1). doi:10.1038/s41597-020-0381-2~~

~~Calafat, F. M., Wahl, T., Tadesse, M. G. & Sparrow, S. N. (2022) Trends in Europe storm surge extremes match the rate of sea-level rise. *Nature* **603**(7903). doi:10.1038/s41586-022-04426-5~~

~~Caldwell, P. C., Merrifield, M. A. & Thompson, P. R. (2015) Sea level measured by tide gauges from global oceans — the Joint Archive for Sea Level holdings (NCEI Accession 0019568), Version 5.5. *NOAA Natl. Centers Environ. Inf.* (18).~~

~~Campos, R. M., Guedes Soares, C., Alves, J. H. G. M., Parente, C. E. & Guimaraes, L. G. (2019) Regional long-term extreme wave analysis using hindcast data from the South Atlantic Ocean. *Ocean Eng.* **179**. doi:10.1016/j.oceaneng.2019.03.023~~

~~Coles, S. (2001) *An Introduction to Statistical Modeling of Extreme Values*. Bristol: Springer.~~

~~Dean, R. & Walton, T. (2010) Wave Setup. In: *Handbook of Coastal and Ocean Engineering*, 1st ed., Vol. 1–2, 1–24. World Scientific Publishing co. doi:10.1142/10353~~

~~Dulac, W., Cattiaux, J., Chauvin, F., Bourdin, S. & Fromang, S. (2023) Assessing the representation of~~

~~tropical cyclones in ERA5 with the CNRM tracker. *Clim. Dyn.* doi:10.1007/s00382-023-06902-8~~

~~Dullaart, J. C. M., Muis, S., Bloemendaal, N., Chertova, M. V., Couasnon, A. & Aerts, J. C. J. H. (2021) Accounting for tropical cyclones more than doubles the global population exposed to low-probability coastal flooding. *Commun. Earth Environ.* **2**(1). doi:10.1038/s43247-021-00204-9~~

~~Environment Agency. (2018) Coastal flood boundary conditions for the UK: 2018 update. Retrieved from https://www.gov.uk/government/publications/coastal-flood-boundary-conditions-for-uk-mainland-and-islands-design-sea-levels~~

~~European Space Agency. (2021) Copernicus Global Digital Elevation Model. *Open Topol.* 1. doi:doi.org/10.5069/G9028PQB~~

~~Fanti, V., Ferreira, Ó., Kümmerer, V. & Loureiro, C. (2023) Improved estimates of extreme wave conditions in coastal areas from calibrated global reanalyses. *Commun. Earth Environ.* **4**(1). doi:10.1038/s43247-023-00819-0~~

~~Frau, R., Andreewsky, M. & Bernardara, P. (2018) The use of historical information for regional frequency analysis of extreme skew surge. *Nat. Hazards Earth Syst. Sci.* **18**(3). doi:10.5194/nhess-18-949-2018~~

~~Haigh, I D, Marcos, M., Talke, S. A., Woodworth, P. L., Hunter, J. R., Hague, B. S., Bradshaw, E., et al. (2021) GESLA Version 3: A major update to the global higher-frequency sea-level dataset. *EarthArXiv* (released), 1–34. Retrieved from https://www.gesla.org.~~

~~Haigh, Ivan D., MacPherson, L. R., Mason, M. S., Wijeratne, E. M. S., Pattiaratchi, C. B., Crompton, R. P. & George, S. (2014) Estimating present day extreme water level exceedance probabilities around the coastline of Australia: Tropical cyclone-induced storm surges. *Clim. Dyn.* **42**(1–2). doi:10.1007/s00382-012-1653-0~~

~~Haigh, Ivan D., Wadey, M. P., Wahl, T., Ozsoy, O., Nicholls, R. J., Brown, J. M., Horsburgh, K., et al. (2016) Spatial and temporal analysis of extreme sea level and storm surge events around the coastline of the UK. *Sci. Data.* doi:10.1038/sdata.2016.107~~

~~Hall, J. A., Gill, S., Obeysekera, J., Sweet, W., Knuuti, K. & Marburger, J. (2016) Regional Sea Level Scenarios for Coastal Risk Management : Managing the Uncertainty of Future Sea Level Change and Extreme Water Levels for Department of Defense Coastal Sites Worldwide (April), 224. Retrieved from https://apps.dtic.mil/sti/citations/AD1013613~~

~~Hamdi, Y., Duluc, C. M., Bardet, L. & Rebour, V. (2016) Use of the spatial extremogram to form a homogeneous region centered on a target site for the regional frequency analysis of extreme storm surges. *Int. J. Saf. Secur. Eng.* **6**(4). doi:10.2495/SAFE-V6-N4-777-781~~

~~Hersbach, H., Bell, B., Berrisford, P., Hirahara, S., Horányi, A., Muñoz-Sabater, J., Nicolas, J., et al. (2020) The ERA5 global reanalysis. *Q. J. R. Meteorol. Soc.* **146**(730), 1999–2049. John Wiley & Sons, Ltd. doi:https://doi.org/10.1002/qj.3803~~

~~Hosking, J. R. M. & Wallis, J. R. (1997) *Regional Frequency Analysis: An approach based on L-moments, Cambridge University Press, New York.* Cambridge Universtiy Press. doi:https://doi.org/10.1017/CBO9780511529443~~

~~India Meteorological Department. (2020) Super Cyclonic Storm Amphan over the southeast Bay of Bengal: Summary. Retrieved from https://internal.imd.gov.in/press_release/20200614_pr_840.pdf~~

~~Irish, J. L., Resio, D. T. & Ratcliff, J. J. (2008) The influence of storm size on hurricane surge. *J. Phys. Oceanogr.* **38**(9). doi:10.1175/2008JPO3727.1~~

~~James, G., Witten, D., Hastie, T. & Tibshirani, R. (2013) *An Introduction to Statistical Learning*. Springer. doi:10.1007/9781461471387~~

~~Knapp, K. R., Kruk, M. C., Levinson, D. H., Diamond, H. J. & Neumann, C. J. (2010) The international best track archive for climate stewardship (IBTrACS). *Bull. Am. Meteorol. Soc.* **91**(3). doi:10.1175/2009BAMS2755.1~~

~~Kumar, S., Lal, P. & Kumar, A. (2021) Influence of Super Cyclone “Amphan” in the Indian Subcontinent amid COVID-19 Pandemic. *Remote Sens. Earth Syst. Sci.* **4**(1–2). doi:10.1007/s41976-021-00048-z~~

~~Liang, B., Gao, H. & Shao, Z. (2019) Characteristics of global waves based on the third-generation wave model SWAN. *Mar. Struct.* **64**. doi:10.1016/j.marstruc.2018.10.011~~

~~Lucas, C., Muraleedharan, G. & Guedes Soares, C. (2017) Regional frequency analysis of extreme waves in a coastal area. *Coast. Eng.* **126**. doi:10.1016/j.coastaleng.2017.06.002~~

~~Lyard, F. H., Allain, D. J., Cancet, M., Carrère, L. & Picot, N. (2021) FES2014 global ocean tide atlas: Design and performance. *Ocean Sci.* **17**(3), 615–649. doi:10.5194/os-17-615-2021~~

~~Marcos, M., Rohmer, J., Vousdoukas, M. I., Mentaschi, L., Cozannet, G. Le & Amores, A. (2019) Increased Extreme Coastal Water Levels Due to the Combined Action of Storm Surges and Wind Waves. *Geophys. Res. Lett.* **46**(8). doi:10.1029/2019GL082599~~

~~McGranahan, G., Balk, D. & Anderson, B. (2007) The rising tide: Assessing the risks of climate change and human settlements in low elevation coastal zones. *Environ. Urban.* **19**(1). doi:10.1177/0956247807076960~~

~~Mitchell, D., Hawker, L., Savage, J., Bingham, R., Lord, N. S., Khan, M. J. U., Bates, P., et al. (2022) Increased population exposure to Amphan-scale cyclones under future climates. *Clim. Resil. Sustain.* **1**(2), 1–16. doi:10.1002/cli2.36~~

~~Mori, N., Yasuda, T., Arikawa, T., Kataoka, T., Nakajo, S., Suzuki, K., Yamanaka, Y., et al. (2019) 2018 Typhoon Jebi post-event survey of coastal damage in the Kansai region, Japan. *Coast. Eng. J.* **61**(3). doi:10.1080/21664250.2019.1619253~~

~~Muis, S., Apecechea, M. I., Dullaart, J., Lima Rego, J. de, Madsen, K. S., Su, J., Yan, K., et al. (2020) A High-Resolution Global Dataset of Extreme Sea Levels, Tides, and Storm Surges, Including Future Projections. *Front. Mar. Sci.* **7**(April), 1–15. doi:10.3389/fmars.2020.00263~~

~~Muis, S., Verlaan, M., Winsemius, H. C., Aerts, J. C. J. H. & Ward, P. J. (2016) A global reanalysis of storm surges and extreme sea levels. *Nat. Commun.* **7**(1), 11969. doi:10.1038/ncomms11969~~

~~Mulet, S., Rio, M. H., Etienne, H., Artana, C., Cancet, M., Dibarboure, G., Feng, H., et al. (2021) The new CNES-CLS18 global mean dynamic topography. *Ocean Sci.* **17**(3), 789–808. doi:10.5194/os-17-789-2021~~

~~Needham, H. F., Keim, B. D. & Sathiaraj, D. (2015) A review of tropical cyclone-generated storm surges: Global data sources, observations, and impacts. *Rev. Geophys.* **53**(2), 545–591. doi:10.1002/2014RG000477~~

~~Neumann, B., Vafeidis, A. T., Zimmermann, J. & Nicholls, R. J. (2015) Future coastal population growth and exposure to sea-level rise and coastal flooding - A global assessment. *PLoS One* **10**(3). doi:10.1371/journal.pone.0118571~~

~~Nicholls, R. J., Lincke, D., Hinkel, J., Brown, S., Vafeidis, A. T., Meyssignac, B., Hanson, S. E., et al. (2021) A global analysis of subsidence, relative sea-level change and coastal flood exposure. *Nat. Clim. Chang.* **11**(4). doi:10.1038/s41558-021-00993-z~~

~~Ramakrishnan, R., Remya, P. G., Mandal, A., Mohanty, P., Arayakandy, P., Mahendra, R. S. & Nair, T. M. B. (2022) Wave induced coastal flooding along the southwest coast of India during tropical cyclone Tauktae. *Sci. Rep.* **12**(1). doi:10.1038/s41598-022-24557-z~~

~~Shaji, C., Kar, S. K. & Vishal, T. (2014) Storm surge studies in the North Indian Ocean: A review. *Indian J. Mar. Sci.* **43**(2).~~

~~Siahsarani, A., Karami Khaniki, A., Aliakbari Bidokhti, A. A. & Azadi, M. (2021) Numerical Modeling of Tropical Cyclone-Induced Storm Surge in the Gulf of Oman Using a Storm Surge–Wave–Tide Coupled Model. *Ocean Sci. J.* **56**(3). doi:10.1007/s12601-021-00027-x~~

~~Slocum, C. J., Razin, M. N., Knaff, J. A. & Stow, J. P. (2022) Does ERA5 mark a new era for resolving the tropical cyclone environment? *J. Clim.* 1–39. doi:10.1175/jcli-d-22-0127.1~~

~~Sweet, W. V., Hamlington, B. D., Kopp, R. E., Weaver, C. P., Barnard, P. L., Bekaert, D., Brooks, W., et al. (2022) Global and Regional Sea Level Rise Scenarios for the United States. *NOAA Tech. Rep. NOS 01* 111 pp. Retrieved from https://oceanservice.noaa.gov/hazards/sealevelrise/noaa-nos-~~

~~Sweet, W. V, Genz, A. S., Obeysekera, J. & Marra, J. J. (2020) A Regional Frequency Analysis of Tide Gauges to Assess Pacific Coast Flood Risk . *Front. Mar. Sci.* . Retrieved from https://www.frontiersin.org/articles/10.3389/fmars.2020.581769~~

~~Taherkhani, M., Vitousek, S., Barnard, P. L., Frazer, N., Anderson, T. R. & Fletcher, C. H. (2020) Sea-level rise exponentially increases coastal flood frequency. *Sci. Rep.* **10**(1). doi:10.1038/s41598-020-62188-4~~

~~Tanim, A. H. & Akter, A. (2019) Storm-surge modelling for cyclone Mora in the northern Bay of Bengal. *Proc. Inst. Civ. Eng. Marit. Eng.* **172**(3). doi:10.1680/jmaen.2019.1~~

~~Timmermans, B. W., Gommenginger, C. P., Dodet, G. & Bidlot, J. R. (2020) Global Wave Height Trends and Variability from New Multimission Satellite Altimeter Products, Reanalyses, and Wave Buoys. *Geophys. Res. Lett.* **47**(9). doi:10.1029/2019GL086880~~

~~Vanem, E. (2017) A regional extreme value analysis of ocean waves in a changing climate. *Ocean Eng.* **144**. doi:10.1016/j.oceaneng.2017.08.027~~

~~Vousdoukas, M. I., Voukouvalas, E., Mentaschi, L., Dottori, F., Giardino, A., Bouziotas, D., Bianchi, A., et al. (2016) Developments in large-scale coastal flood hazard mapping. *Nat. Hazards Earth Syst. Sci.* **16**(8). doi:10.5194/nhess-16-1841-2016~~

~~Wang, J. & Wang, Y. (2022) Evaluation of the ERA5 Significant Wave Height against NDBC Buoy Data from 1979 to 2019. *Mar. Geod.* **45**(2). doi:10.1080/01490419.2021.2011502~~

~~Weiss, J. & Bernardara, P. (2013) Comparison of local indices for regional frequency analysis with an application to extreme skew surges. *Water Resour. Res.* **49**(5). doi:10.1002/wrcr.20225~~

~~Yang, Z., Wang, T., Castrucci, L. & Miller, I. (2020) Modeling assessment of storm surge in the Salish Sea. *Estuar. Coast. Shelf Sci.* **238**. doi:10.1016/j.ecss.2019.106552~~

8. Appendix

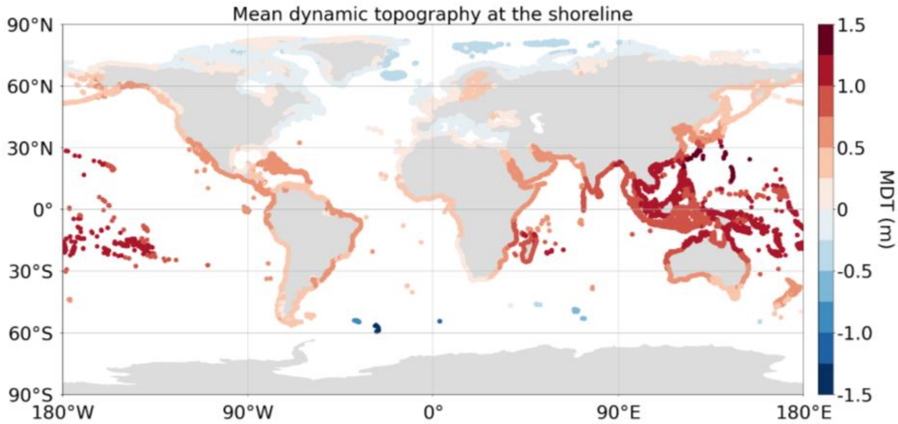

Figure A1: HYBRID-CNES-CLS18-CMEMS2020 MDT dataset from Mulet et al., (2021), extracted at the shoreline for use in correcting the output from the RFA for future uses such as inundation modelling.

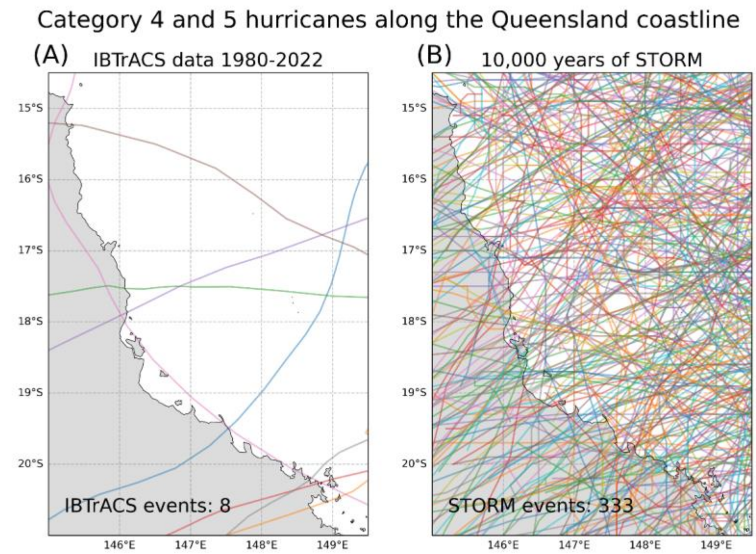

Figure A2: (A) Category 4 and 5 IBTrACS hurricane impacting the Queensland coastline between 1980-2022 (Knapp et al., 2010) and (B) equivalent STORM events impacting the same the stretch of coastline (Bloemendaal et al., 2020).

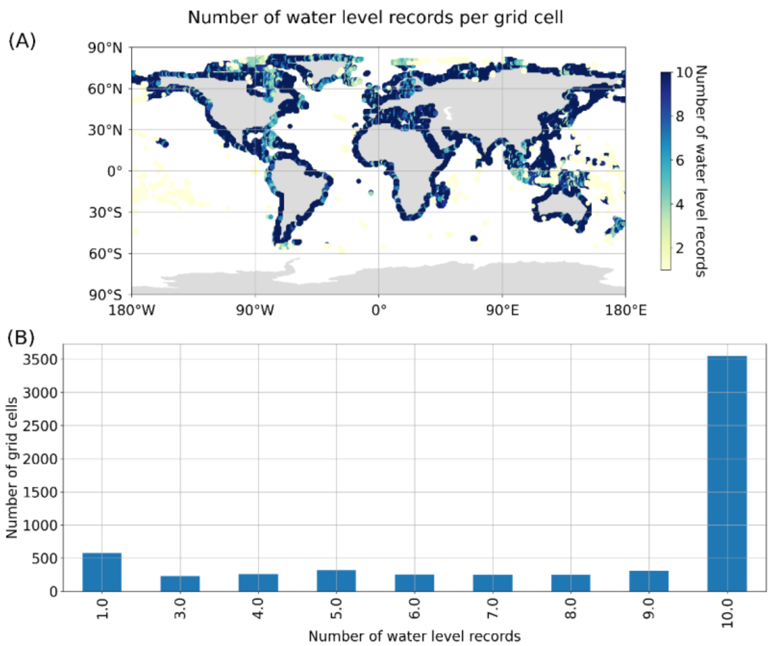

Figure A3: The number of water level records used per grid cell (A) as a scatter plot showing the distribution globally, and (B) as a bar plot showing the number of water level records vs the number of grid cells.

Formatted: Keep with next

Formatted: Caption

9. Code Availability

The Python scripts used for handling the GESLA dataset can be downloaded for: https://github.com/philiprt/GeslaDataset

The Conda package (Python) used for creating the FES2014 tidal timeseries can found at: https://anaconda.org/fbriol/pyfes

10. Data availability

GESLA tide gauge data is available at: https://gesla787883612.wordpress.com/downloads/

GTSM data is available at: https://cds.climate.copernicus.eu/cdsapp#!/dataset/sis-water-level-change-timeseries?tab=overview

ERA5 wave hindcast data is available at: https://cds.climate.copernicus.eu/cdsapp#!/dataset/reanalysis-era5-single-levels?tab=overview

FES2014 tidal heights can be downloaded from:

https://www.aviso.altimetry.fr/en/data/products/auxiliary-products/global-tide-fes.html

HYBRID-CNES-CLS18-CMEMS2020 is available at:

https://www.aviso.altimetry.fr/en/data/products/auxiliary-products/mdt/mdt-global-hybrid-cnes-cls-cmems.html

Copernicus 30m DEM is found at: https://spacedata.copernicus.eu/collections/copernicus-digital-elevation-model

COAST-RP dataset is downloaded from: https://data.4tu.nl/articles/_/13392314

The data produced in this study is available for academic, non-commercial research only. Please contact the corresponding author for access.

11. Author contributions

T.C. was responsible for coding up the pre-processing the tide gauge and GTSM data, coding up the RFA and validating the results. N.Q. pre-processed the wave data, including fitting the copula to predict wave conditions for tide gauge records that extended beyond the hindcast period. J.G. created the coastline output points using the Copernicus DEM. I.P. worked on the evaluating the empirical shape parameter limiter. H.W. assisted in validating the output results from the RFA. S.M. supplied the GTSM dataset and W.S. provided the RFA methodology which we applied globally. I.H. and P.B. provided guidance and assistance throughout. T.C. prepared the manuscript with contributions and editing from all co-authors.

12. Competing Interests

The authors declare that they have no conflict of interest.